

# Predictability of the 2020 Antarctic strong vortex event and the role of ozone forcing

Eun-Pa Lim<sup>1</sup>, Linjing Zhou<sup>2</sup>, Griffith A Young<sup>2</sup>, Abhik Santra<sup>3</sup>, Irina Rudeva<sup>2</sup>, Pandora Hope<sup>2</sup>, Matthew Comstock Wheeler<sup>1</sup>, Julie M. Arblaster<sup>4</sup>, Harry H. Hendon<sup>2</sup>, Gloria L Manney<sup>5</sup>, Seok-Woo Son<sup>6</sup>, and Jiyoung Oh<sup>6</sup>

<sup>1</sup>Bureau of Meteorology (Australia)

<sup>2</sup>Bureau of Meteorology

<sup>3</sup>Bureau of Meteorology, Melbourne, Australia

<sup>4</sup>Monash University

<sup>5</sup>Northwest Research Associates

<sup>6</sup>Seoul National University

February 23, 2024

## Abstract

In the austral spring seasons of 2020-2022, the Antarctic stratosphere experienced three consecutive strong vortex events. In particular, the Antarctic vortex of October-December 2020 was the strongest on record in the satellite era for that season at 60°S in the mid- to lower stratosphere. However, it was poorly predicted by the Australian Bureau of Meteorology's operational seasonal climate forecast system of that time, ACCESS-S1, even at a short lead time of a month. Using the current operational forecast system, ACCESS-S2, we have, therefore, tried to find a primary cause of the limited predictability of this event and conducted forecast sensitivity experiments to climatological versus observation-based ozone to understand the potential role of the ozone forcing in the strong vortex event and associated anomalies of the Southern Annular Mode (SAM) and south-eastern Australian rainfall. Here, we show that the 2020 strong vortex event did not follow the canonical dynamical evolution seen in previous strong vortex events in spring, whereas the ACCESS-S2 control forecasts with the climatological ozone did, which likely accounts for the inaccurate forecasts of ACCESS-S1/S2 at 1-month lead time. Forcing ACCESS-S2 with observed ozone significantly improved the skill in predicting the strong vortex in October-December 2020 and the subsequent positive SAM and related rainfall increase over south-eastern Australia in the summer of December 2020 to February 2021. These results highlight an important role of ozone variations in seasonal climate forecasting as a source of long-lead predictability, and therefore, a need for improved ozone forcing in future ACCESS-S development.

## Hosted file

LimEtAl\_2024\_JGR.docx available at <https://authorea.com/users/745281/articles/717419-predictability-of-the-2020-antarctic-strong-vortex-event-and-the-role-of-ozone-forcing>

# 1 Predictability of the 2020 Antarctic strong vortex 2 event and the role of ozone forcing 3

4 Eun-Pa Lim<sup>1</sup>, Linjing Zhou<sup>1</sup>, Griffith Young<sup>1</sup>, S. Abhik<sup>2</sup>, Irina Rudeva<sup>1</sup>, Pandora Hope<sup>1</sup>, Matthew C.  
5 Wheeler<sup>1</sup>, Julie M. Arblaster<sup>3</sup>, Harry H. Hendon<sup>3</sup>, Gloria L. Manney<sup>4,5</sup>, Seok-Woo Son<sup>6</sup>, Jiyoung Oh<sup>7</sup>

6 <sup>1</sup> Bureau of Meteorology, Melbourne, Victoria, Australia

7 <sup>2</sup> School of Earth, Atmosphere and Environment, Monash University, Clayton, Victoria, Australia

8 <sup>3</sup> Securing Antarctica's Environmental Future, School of Earth, Atmosphere and Environment,  
9 Monash University, Clayton, Victoria, Australia

10 <sup>4</sup> NorthWest Research Associates, Socorro, New Mexico, USA

11 <sup>5</sup> Department of Physics, New Mexico Institute of Mining and Technology, Socorro, New Mexico,  
12 USA

13 <sup>6</sup> School of Earth and Environmental Sciences, Seoul National University, Seoul, Republic of Korea

14 <sup>7</sup> Korea Meteorological Administration, Seoul, Republic of Korea  
15

16 Corresponding author: Eun-Pa Lim, [eun-pa.lim@bom.gov.au](mailto:eun-pa.lim@bom.gov.au)  
17

## 18 **Key points**

- 19 • The Antarctic vortex of 2020 was the strongest event in the satellite era for the October-  
20 December mean in the mid- to lower stratosphere
- 21 • Its unusual dynamical evolution limited its predictability to less than a month
- 22 • Realistic ozone forcing could significantly improve forecasts for the 2020 polar vortex  
23 strength and its downward impact

24

## 25 Abstract

26 In the austral spring seasons of 2020-2022, the Antarctic stratosphere experienced three consecutive  
27 strong vortex events. In particular, the Antarctic vortex of October-December 2020 was the strongest  
28 on record in the satellite era for that season at 60°S in the mid- to lower stratosphere. However, it was  
29 poorly predicted by the Australian Bureau of Meteorology's operational seasonal climate forecast  
30 system of that time, ACCESS-S1, even at a short lead time of a month. Using the current operational  
31 forecast system, ACCESS-S2, we have, therefore, tried to find a primary cause of the limited  
32 predictability of this event and conducted forecast sensitivity experiments to climatological versus  
33 observation-based ozone to understand the potential role of the ozone forcing in the strong vortex  
34 event and associated anomalies of the Southern Annular Mode (SAM) and south-eastern Australian  
35 rainfall. Here, we show that the 2020 strong vortex event did not follow the canonical dynamical  
36 evolution seen in previous strong vortex events in spring, whereas the ACCESS-S2 control forecasts  
37 with the climatological ozone did, which likely accounts for the inaccurate forecasts of ACCESS-  
38 S1/S2 at 1-month lead time. Forcing ACCESS-S2 with observed ozone significantly improved the  
39 skill in predicting the strong vortex in October-December 2020 and the subsequent positive SAM and  
40 related rainfall increase over south-eastern Australia in the summer of December 2020 to February  
41 2021. These results highlight an important role of ozone variations in seasonal climate forecasting as a  
42 source of long-lead predictability, and therefore, a need for improved ozone forcing in future  
43 ACCESS-S development.

## 44 Plain Language Summary

45 In the spring seasons of 2020-2022, the Antarctic stratosphere experienced three strong vortex events.  
46 In particular, the Antarctic vortex of October-December 2020 was the strongest on record in the  
47 satellite observation era for that season when monitored at 60°S in the mid- to lower stratosphere  
48 (altitudes of 15-30 km). However, this super vortex event was poorly predicted by the Australian  
49 Bureau of Meteorology's operational seasonal climate forecast system even at 1-month lead time. Our  
50 analysis reveals that the dynamical evolution of the 2020 polar vortex was highly unusual compared  
51 to those of the previous strong vortex events, which likely explains its lack of long-lead predictability.  
52 The forecast model experiments prescribed with observed versus unrealistic ozone forcing show that  
53 using the observed ozone, characterized by a significant loss over Antarctica in spring 2020, resulted  
54 in the forecast improvements for the 2020 super vortex strength and the associated poleward shift of  
55 the Southern Hemisphere (SH) midlatitude jet in the lower atmosphere and anomalously wet  
56 conditions over south-eastern Australia in summer. These results highlight a need to improve  
57 representations of ozone forcing in dynamical sub-seasonal to seasonal climate forecast systems to  
58 better predict the year-to-year variability of the SH surface climate conditions.

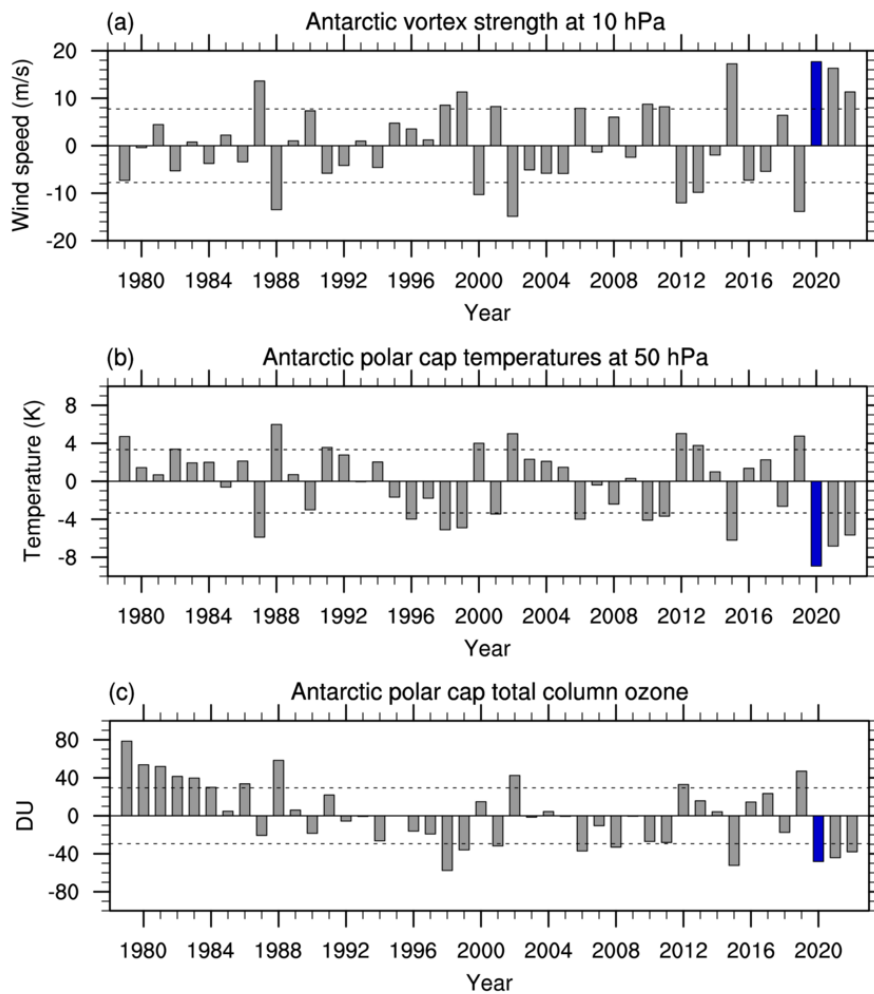
## 59 1. Introduction

60 The Antarctic stratospheric polar vortex (also referred to as the polar vortex in this study) is a  
61 planetary-scale cyclonic circulation encircling the South Pole from austral autumn to spring. Its  
62 maximum westerly wind speed is found in the latitude band of 40-50°S near the stratopause (~1 hPa  
63 level) in winter (Andrews et al., 1987), and as the season progresses through spring, it gradually  
64 weakens with poleward and downward movements as a result of vigorous wave-mean flow  
65 interactions (e.g., Matsuno 1970; Hartmann et al. 1984; Randel and Newman 1998). Eventually, the  
66 westerly vortex breaks down sometime in November to December in the upper to mid-stratosphere  
67 (Black & McDaniel, 2007; Hio & Yoden, 2005; Kuroda & Kodera, 1998).

68 The interannual variability of the Antarctic stratospheric vortex peaks in the upper to mid-stratosphere  
69 in October and is often the expression of different paces of the seasonal march of the vortex (e.g.,  
70 Shiotani et al. 1993; Byrne and Shepherd 2018). Active feedback between planetary-scale waves and  
71 vortex winds on latitudinal and vertical critical lines (where the phase speeds of waves equal the  
72 background zonal wind speeds) leads to poleward and downward movements of the anomalous wind,  
73 temperature, and pressure around and over the Antarctic region (e.g., Kuroda and Kodera 1998; Hio  
74 and Yoden 2005; Shaw et al. 2010; Byrne and Shepherd 2018; Lim et al. 2018). The downward  
75 coupling of the stratospheric anomalies with some time lag makes the Antarctic stratospheric vortex  
76 variability during spring and early summer an important source of predictability of the state of the  
77 tropospheric Southern Annular Mode (SAM) (e.g., Kidson 1988; Gong and Wang 1999; Thompson  
78 and Wallace 2000; Marshall 2003); which, in turn, significantly impacts Southern Hemisphere (SH)  
79 surface weather and climate as well as associated oceanic circulations and sea-ice extent (e.g.,  
80 Silvestri and Vera 2003; Reason and Rouault 2005; Sen Gupta and England 2006; Gillett et al. 2006;  
81 Hendon et al. 2007, 2014; Stammerjohn et al. 2008; Harris and Lucas 2019; Lim et al. 2019; Wang et  
82 al. 2019; Hartmann 2022). For instance, when the seasonal march of the vortex evolution is  
83 accelerated, the spring polar vortex weakens and warms earlier than usual. Weaker and warmer polar  
84 vortices can lead to unusually high Antarctic ozone concentrations, which further warm the Antarctic  
85 region, and consequently result in the SAM to be in its negative phase in spring through early summer  
86 (e.g., years 2002, 2019) (Stolarski et al. 2005; Byrne and Shepherd 2018; Lim et al. 2018; Noguchi et  
87 al. 2020). The opposite chain of processes occurs when the seasonal march of the vortex evolution is  
88 decelerated, and the spring vortex is unusually strong and cold and breaks down later than usual  
89 (Limpasuvan et al., 2005).

90 Previous studies noted that the interannual variability of the Antarctic stratospheric vortex has  
91 significantly increased since 2000 (E.-P. Lim et al., 2018; Shen et al., 2022), a period when the Inter-  
92 decadal Pacific Oscillation has been in its cold phase (e.g., Yuan Zhang et al. 1997; Kosaka and Xie  
93 2013; Henley et al. 2015) and a plateauing or weak recovery of the Antarctic ozone depleting trend

94 has been detected (e.g., Salby et al. 2011; Solomon et al. 2016; Stone et al. 2021). In particular, the  
 95 springtime Antarctic polar vortex experienced its full swing from a near-record/record-breaking  
 96 vortex weakening and warming event in 2019 to three consecutive strong and cold vortex events in  
 97 2020-2022 (e.g., Rao et al. 2020; Shen et al. 2020; Wargan et al. 2020; Lim et al. 2021; Yook et al.  
 98 2022). The strong and persistent 2020 vortex in late spring was especially noteworthy as it was the  
 99 strongest and coldest event since at least 1979 in the mid- to lower stratosphere for the October to  
 100 December mean (Figs. 1a,b). The Antarctic ozone concentration was also significantly lower than  
 101 normal during that season (Fig. 1c), as expected from the exceptionally strong and more persistent  
 102 polar vortex (e.g.,



103

104 **Figure 1.** (a) Time series of the October-December mean stratospheric polar vortex wind anomalies as  
 105 monitored by zonal-mean zonal wind anomalies ( $[U]$ ) relative to the climatology of 1981-2018 at 60°S and 10  
 106 hPa. (b) The same as (a) but temperature anomalies averaged over the Antarctic polar cap region poleward of  
 107 60°S at 50 hPa. (c) The same as (a) but total column ozone anomalies averaged over the Antarctic polar cap  
 108 region poleward of 63°S. The 2020 anomalies are marked by the blue-colored bars. The horizontal lines denote  
 109  $\pm 1$  standard deviation ( $\sigma$ ). The wind and temperature data are from the JRA-55 reanalysis (Kobayashi et al., 2015)  
 110 and the ozone data are from the NASA Ozone Watch (<https://ozonewatch.gsfc.nasa.gov/SH.html>).

111 Randel and Newman 1998; Seviour et al. 2014; Lim et al. 2018). Although this low polar cap ozone  
 112 anomaly came after an unusual wintertime ozone depletion in the lower latitudes of the SH caused by  
 113 the Australian Black Summer (or Australian New Year's) bushfire smoke of late 2019 to early 2020  
 114 (Rieger et al. 2021; Yu et al. 2021; Santee et al. 2022; Solomon et al. 2023), the studies of Santee et al.  
 115 (2022) and Solomon et al. (2023) indicate that the austral springtime ozone loss of 2020 over  
 116 Antarctica did not result from the smoke.

117 Despite its record strength, the 2020 super vortex event was not well predicted by the Bureau of  
 118 Meteorology (BoM)'s operational dynamical sub-seasonal to seasonal (S2S) climate forecast system,  
 119 ACCESS-S1 (the Australian Community Climate and Earth System Simulator – Seasonal version 1;  
 120 Hudson et al. 2017), until the beginning of October 2020, by which time the anomalously strong  
 121 vortex condition had already persisted for a month (Fig. 2). The lack of long-lead predictability of this  
 122 super vortex event was puzzling because dynamical S2S forecast systems demonstrate useful skill in  
 123 predicting the SH spring stratospheric polar vortex from July when assessed over their hindcast  
 124 periods of 20-40 years (E. P. Lim et al., 2021; Wedd et al., 2022). Consistent with the hindcast skill,  
 125 ACCESS-S1 and S2 skilfully predicted the 2021 and 2022 Antarctic strong vortex events of October-  
 126 December, respectively, at 2-month lead time from early August (Supplementary Fig. S1). One  
 127 contributor to the poor forecast performance for the 2020 vortex event could be that the forecasts were  
 128 forced by prescribed unrealistic ozone concentrations (i.e., the monthly climatological ozone as a  
 129 common forecast practice) (e.g., Seviour et al. 2014; Hendon et al. 2020; Oh et al. 2022) rather than  
 130 being forced by dynamically balanced more realistic ozone concentrations (e.g., as simulated by an  
 131 interactive chemistry-climate model; Fogt et al. 2009, Friedel et al. 2022). In this study, we aim to  
 132 understand i) some key characteristics of the 2020 super vortex event that could be related to its lack  
 133 of predictability at a lead time as short as 1 month; and ii) the role of the ozone forcing in the strength  
 134 of the polar vortex and its downward impact on the surface SAM and associated Australian rainfall,  
 135 which should highlight the interannual variability of ozone as a potential source of predictability of  
 136 this strong vortex event and associated SH surface climate anomalies.

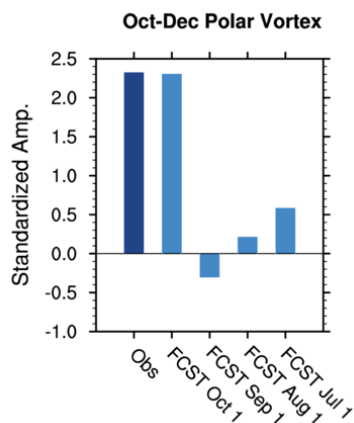


**Figure 2.** ACCESS-S1 11- member ensemble mean forecasts for the October-December mean stratospheric polar vortex ( $[U]$  at 60°S, 10 hPa) when forecasts were initialised on 1 October (lead time 0), 1 September (lead time 1 month), 1 August (lead time 2 months), and 1 July (lead time 3 months) of 2020 (light blue bars). The dark blue bar indicates the observed strength of the 2020 vortex. The observed and forecast standardized anomalies were obtained relative to their respective climatological means and standard deviations of 1990-2012 (when ACCESS-S1 hindcasts are available).

137

## 138 2. Data, forecast system, and experimental design

139 To address the above research questions, we have conducted forecast sensitivity experiments to  
140 climatological vs. realistic 2020 ozone forcing, using the BoM's S2S forecast system, ACCESS-S2,  
141 which replaced ACCESS-S1 as the operational system in October 2021 (Wedd et al. 2022). ACCESS-  
142 S2 is an atmosphere-land-ocean-sea-ice fully coupled dynamical forecast system. Its model is based  
143 on the UK Met Office GloSea5-GC2 seasonal prediction system (MacLachlan et al., 2015) and is  
144 identical to ACCESS-S1 except for minor corrections and enhancements, including a correction in the  
145 atmospheric model code that reads ozone data to follow a 365-day calendar instead of a 360-day  
146 calendar (Hendon et al., 2020; Wedd et al., 2022). The model's horizontal resolution is 25 km in the  
147 ocean and ~60 km in the atmosphere in the midlatitudes (N216). The vertical resolution of the  
148 atmospheric model (the Unified Model version 8.6; Walters et al. 2017) is 85 levels with a well-  
149 resolved stratosphere (35 levels above 18 km). The main difference between ACCESS-S1 and  
150 ACCESS-S2 is that ACCESS-S2 is initialized using the BoM's weakly-coupled ensemble optimum  
151 interpolation data assimilation scheme for the ocean, sea-ice, and land surface (Wedd et al., 2022). In  
152 contrast, ACCESS-S1 was initialized with the UK Met Office Forecast Ocean Assimilation Model  
153 (FOAM) analysis data (J. Waters et al., 2015). The ocean initial conditions for ACCESS-S2 are  
154 available for 1981-2018 and October 2021 onwards. Due to the unavailability of these new conditions  
155 for 2020, we used the UK Met Office FOAM analysis data (J. Waters et al., 2015) to initialise our  
156 experiments. The atmospheric initial conditions come from the BoM's 4-D Var data assimilation  
157 analyses for 2020 (Bureau of Meteorology, 2019) and the European Centre for Medium-Range  
158 Weather Forecasts (ECMWF)-Interim reanalysis (ERA-Interim; Dee et al. 2011) for the hindcasts  
159 (retrospective forecasts) for 1981-2018.

160 For this study, we generated 3-member hindcasts for 1981-2018 to compute the forecast climatology  
161 and 33-member ensemble forecasts for 2020 by perturbing the atmospheric initial conditions (Hudson  
162 et al. 2017; Wedd et al. 2022). These forecasts were forced with prescribed monthly *climatological*  
163 zonal-mean ozone averaged over 1994-2005 (Cionni et al., 2011), the same as the operational  
164 configuration of ACCESS-S2 (and ACCESS-S1) for ozone forcing. We refer to these standard  
165 forecasts as the “control” forecasts. To understand the role of the 2020 ozone forcing in the strength  
166 of the polar vortex and its downward impacts, we generated a second set of 33-member ensemble  
167 forecasts forced with the prescribed *2020 observed* monthly zonal-mean ozone from the ECMWF  
168 Reanalysis version 5 (ERA5; Hersbach et al. 2020). ERA5 assimilates more and higher quality  
169 observational data compared to its predecessor (Dee et al., 2011), including assimilation of Aura  
170 Microwave Limb Sounder (J. W. Waters et al., 2006) Ozone Profiles and Ozone Monitoring  
171 Instrument column ozone (Levelt et al., 2006), which provide near-global daily coverage. ERA5  
172 stratospheric ozone has been demonstrated to be accurate by comparisons with observational data and  
173 other reanalyses (e.g., SPARC 2022, Chapter 4). The ERA5 ozone anomalies for 2020 were computed

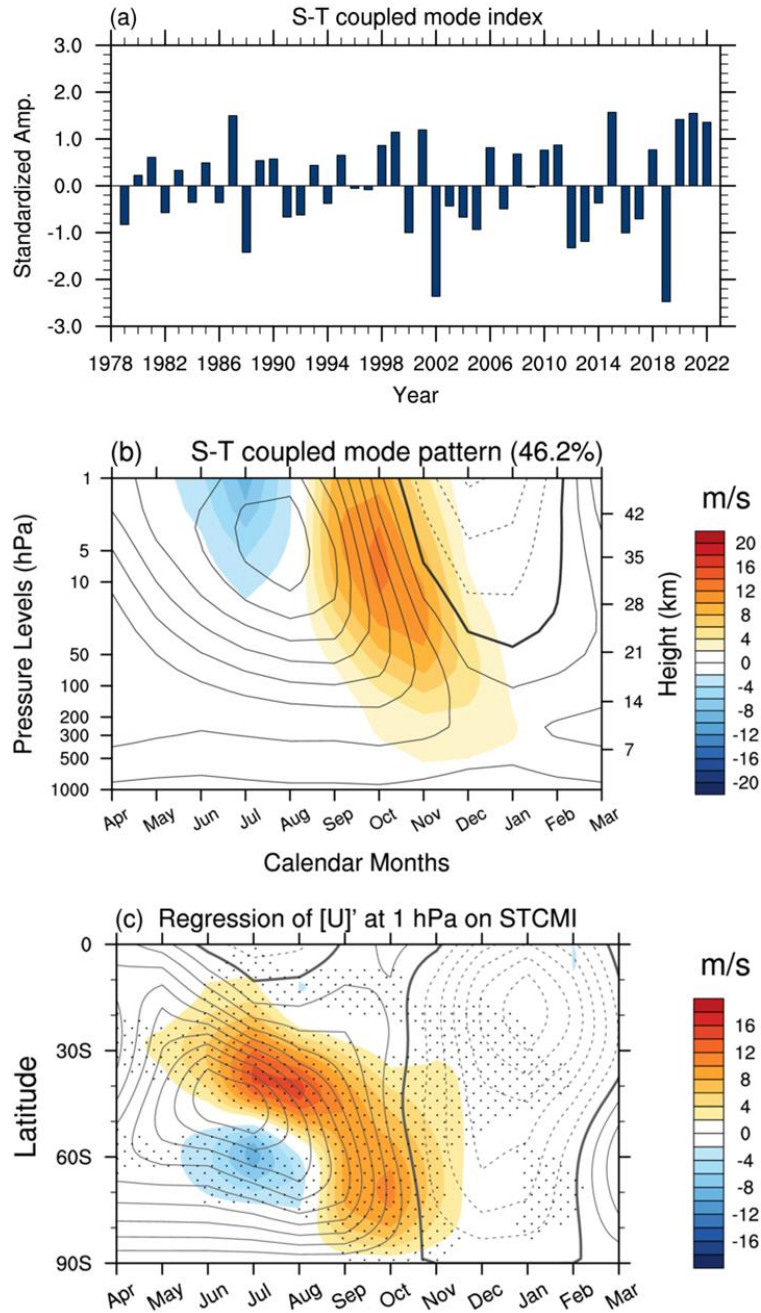
174 relative to the ERA5 climatology of 1994-2005 and then added to the ozone climatology used for the  
175 control forecasts throughout all vertical levels. These forecasts are referred to as the "experimental"  
176 forecasts.

177 All forecasts were initialized on 1 September 2020 and verified from September 2020 to February  
178 2021. The forecasts are verified against the JRA-55 data (the Japanese 55-year ReAnalysis;  
179 Kobayashi et al. 2015). The JRA-55 reanalysis dataset has been shown to be of high quality for  
180 dynamics studies such as those herein (e.g., SPARC, 2022, Chapter 6). However, it does not do inline  
181 ozone assimilation (Hersbach et al., 2020). The rainfall forecasts over Australia are verified against  
182 the BoM's Australian Gridded Climate Data (AGCD; Jones et al. 2009; Evans et al. 2020).

### 183 3. Characteristics of the observed 2020 super vortex event and ozone anomalies

184 Year-to-year variability of the polar vortex in the reanalysis data is identified by an empirical  
185 orthogonal function (EOF) analysis (North et al., 1982) applied to the zonal-mean zonal wind  
186 anomalies ( $[U]$ ) at 60°S over the domain of vertical (pressure) levels and calendar months (Figs. 3a,b)  
187 (e.g., Hio and Yoden 2005; Lim et al. 2018). The interannual variability is characterized by persistent  
188 anomalies during spring and early summer throughout the stratosphere and the troposphere, with a  
189 maximum anomaly in the mid- to upper stratosphere in October. These anomalies, when positive, are  
190 related to a delay of the vortex breakdown in the upper to mid-stratosphere (and an earlier breakdown  
191 when negative). The other notable feature in Figure 3b is the oppositely signed wind anomalies in the  
192 upper stratosphere during the austral winter months that precede wind anomalies of spring and early  
193 summer.

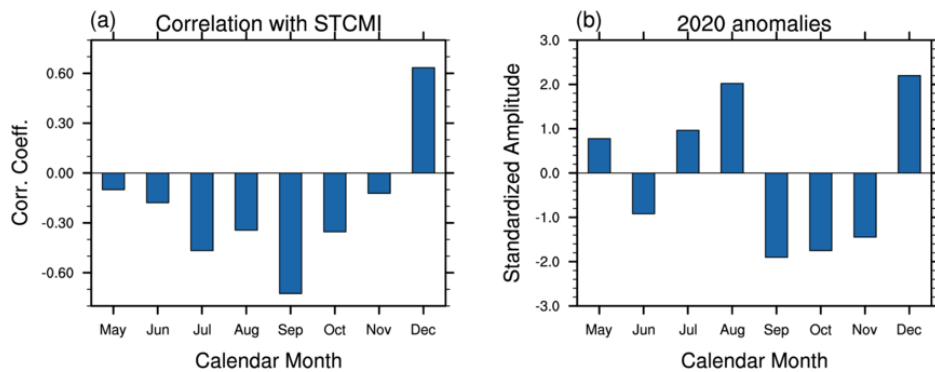
194 Dynamical processes associated with this abrupt change of upper stratospheric zonal wind anomalies  
195 at around 60°S from winter to spring can be understood by examining the zonal wind anomalies at 1  
196 hPa regressed to the temporal coefficients of the EOF pattern (Fig. 3a) displayed as a function of the  
197 latitude and calendar months (Fig. 3c). The regression plot shows that the negative zonal wind  
198 anomalies at 60°S in June and July displayed in Figure 3b are associated with an equatorward shift of  
199 the winter jet in the upper stratosphere as marked by the meridional dipole anomalies centered on the  
200 jet. The dipole anomalies of the winter jet gradually move poleward with time as a result of active  
201 interactions with the upward and equatorward propagation of planetary-scale waves and associated  
202 wave breaking at the critical latitudes (e.g., Hartmann et al. 1984; Kuroda and Kodera 1998; Polvani  
203 and Waugh 2004; Lim et al. 2018, 2021; Baldwin et al. 2021). This wave-mean flow feedback that



204

205 **Figure 3.** The stratosphere-troposphere (S-T) coupled mode captured by the first mode of a height-time domain  
 206 EOF analysis applied to the monthly mean zonal mean-zonal wind anomalies ( $[U]'$ ) at  $60^{\circ}\text{S}$  over 1979-2022. (a)  
 207 The S-T coupled mode temporal coefficient time series (S-T coupled mode index; STCMI), (b) the S-T coupled  
 208 mode eigenvector (EOF1), and (c) regression of  $[U]'$  at 1 hPa onto the STCMI displayed in (a) (regression  
 209 coefficients were scaled by  $1\sigma$  of the STCMI to preserve the wind unit). The contours in (b) and (c) indicate the  
 210 1981-2018 climatology of  $[U]$  at  $60^{\circ}\text{S}$  and  $[U]$  at 1 hPa, respectively. The thin-solid, thick-solid and thin-dashed  
 211 lines indicate positive, zero and negative zonal mean winds, respectively. The contour interval is  $10\text{ ms}^{-1}$ .  
 212 Stippling in (c) denotes statistically significant regression coefficients at the 90% confidence level, as assessed  
 213 by a two-tailed student t-test with 44 samples.

214 leads to a spring polar vortex anomaly can be summarized by simple statistical relationships as shown  
 215 in Lim et al. (2021): the June-July mean westerly wind anomalies at 60°S and 1 hPa are positively  
 216 correlated with the July-August mean upward propagating wave activities represented by the  
 217 poleward eddy heat flux ( $-v'T'$  in the SH) anomalies averaged over 45-75°S at 100 hPa (correlation  
 218 coefficient,  $r \sim 0.5$ ). These late winter wave activities are, in turn, anti-correlated with the September-  
 219 November mean  $[U]$  at 60°S and 10 hPa ( $r \sim -0.6$ ). Consequently, the spring zonal wind anomalies  
 220 are anti-correlated with the early winter westerly anomalies at 60°S and 1 hPa ( $r \sim -0.6$ ), as depicted  
 221 in Figure 3b. Because of these time-lagged relationships, the winter jet dipole anomalies in the upper  
 222 stratosphere and the upward propagating wave activity anomalies in the lower stratosphere are  
 223 important precursors that serve as sources of predictability of the springtime polar vortex condition  
 224 (e.g., Shiotani et al. 1993; Polvani and Waugh 2004). Thus, an unusually strong springtime polar  
 225 vortex often follows from stronger wintertime westerlies in midlatitudes and weaker westerlies in high  
 226 latitudes at the top of the stratosphere (i.e., an equatorward shift of the winter upper-stratospheric jet;  
 227 Shiotani et al. 1993). Such changes in the zonal winds tend to discourage planetary-scale waves  
 228 propagating into the stratosphere during winter months (as measured by reduced poleward heat flux at  
 229 100 hPa in the SH) (Fig. 4a).



230  
 231 **Figure 4.** (a) Correlation of poleward eddy heat flux detected at 100 hPa with the STCMI displayed in Figure 3a.  
 232 Negative correlation means less heat is transported poleward and upward (i.e., reduced upward propagating  
 233 wave activity) in relation to the stronger-than-normal zonal winds in spring to early summer. (Note that in the SH,  
 234 the *poleward* heat flux is computed as  $-v'T'$  where  $v'$  and  $T'$  are the eddy components of meridional wind and  
 235 temperature, respectively - i.e., *negatively signed northward* heat flux). 0.3 correlation is statistically significant at  
 236 the 95% confidence level as assessed by a two-tailed student t-test with 44 samples from 1979-2022. (b) Monthly  
 237 mean anomalies of 2020 poleward eddy heat flux.

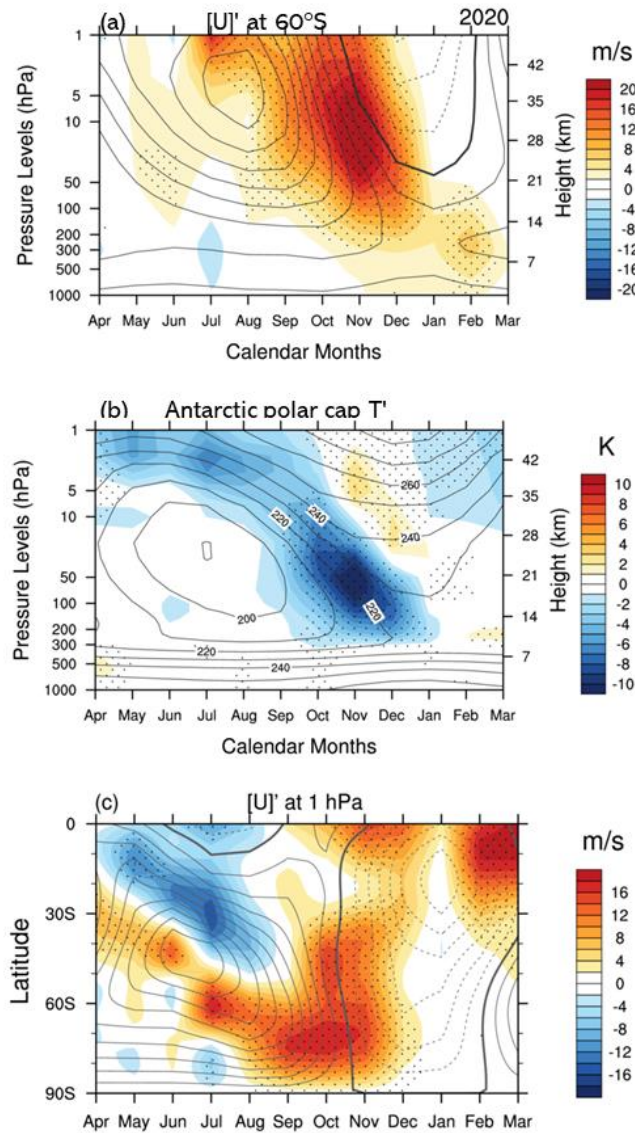
238 In comparison to this canonical process, in 2020 the stronger-than-normal zonal-mean zonal winds  
 239 around 60°S in the upper stratosphere were extraordinarily persistent from May until December (Fig.  
 240 5a). The westerly anomalies of the vortex in the upper stratosphere in July showed signs of a decrease  
 241 in August and September. However, they increased again from October, in contrast to the typical  
 242 evolution of the polar vortex, which would be a continuing decrease of the westerlies in spring (as  
 243 implied in Figure 3b). Further, the vortex wind anomaly of 2020 peaked in November in the mid-

244 stratosphere, later in time and lower in altitude than the variability maximum. The unusually strong  
245 vortex wind anomalies were accompanied by significant cold anomalies in the Antarctic vortex (Fig.  
246 5b). The unconventional dynamical evolution of this super vortex event is also apparent in the latitude-  
247 time plot of the 2020 [U]' at 1 hPa in Figure 5c. The winter stratospheric jet had easterly anomalies on  
248 its equatorward side and westerly anomalies on its poleward side, suggesting a poleward shift of the  
249 jet (i.e., poleward shrinking of the vortex), which would generally lead to spring polar vortex  
250 weakening as implied in Figure 3c (with the opposite signs). Consistent with this poleward winter jet  
251 shift, there was an increase in the poleward eddy heat flux in the lower stratosphere in July and August  
252 (Fig. 4b), which implies increased heat transport toward the polar region and upward propagating  
253 wave activities that would act to weaken the polar vortex in spring. Therefore, the wintertime winds  
254 and wave forcing in 2020 appeared favorable for an anomalous weakening of the springtime polar  
255 vortex, which suggests that the unusual vortex strength in October-December was unlikely to be the  
256 result of canonical dynamical forcing that typically comes from the upper stratosphere in winter (E.-P.  
257 Lim et al., 2018; E. P. Lim et al., 2021). In contrast, the upper stratospheric dynamical evolution of the  
258 unusually strong vortices of October-December 2021 and 2022 was consistent with that historically  
259 associated with stronger-than-normal spring polar vortices, as shown in Figure 3c (Fig. S2).

260 Although the unusually strong polar vortex of 2020 occurred without an obvious dynamical precursor,  
261 its wind and temperature anomalies moved downward to the surface in a typical manner, thereby  
262 likely contributing to the positive SAM that developed in the late spring and summer months of  
263 November-February, when the 2020-21 La Niña would have also played a role in promoting a  
264 positive SAM (e.g., L'Heureux and Thompson 2006; Lim and Hendon 2015; Fogt and Marshall 2020)  
265 (Fig. 6). The positive SAM was likely a key driver of the unusually wet conditions over south-eastern  
266 Australia during austral summer 2020-21, given its resemblance to the historical response of the  
267 summer rainfall to the positive SAM (e.g., Hendon et al. 2007; Fig. 7). On the other hand, the  
268 excessive rainfall over northern and western Australia was likely driven by La Niña combined with a  
269 long-term tropical SST trend (e.g., McBride and Nicholls 1983; Risbey et al. 2009; Lim et al. 2016;  
270 Sharmila and Hendon 2020; Heidemann et al. 2023).

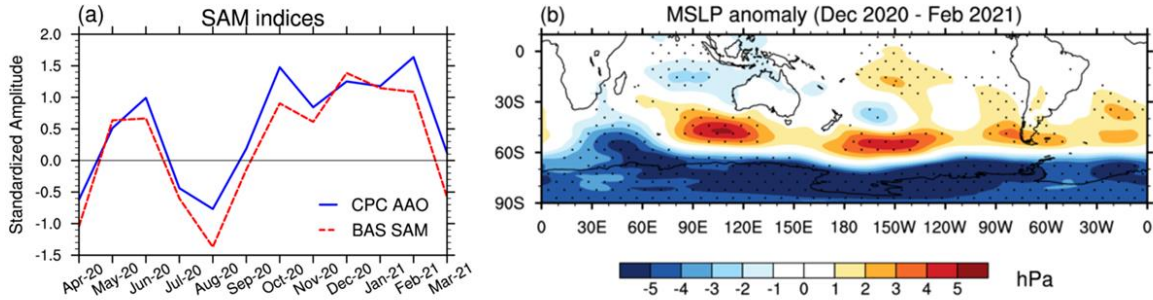
271 As briefly discussed in the introduction, the Antarctic ozone in the lower stratosphere was  
272 significantly less than normal from September 2020 to the following year's January, reflecting the  
273 ozone being extensively depleted in early spring by the unusually strong and cold polar vortex and  
274 then staying confined within the vortex until the vortex broke down in early summer (Fig. 8a). Near  
275 the tropopause, the lower-than-usual Antarctic ozone concentration appears to have lingered at least  
276 until March 2021. Also, the anomalous ozone depletion in winter 2020 in the midlatitudes near 30-  
277 50°S is apparent at 50 hPa (Fig. 8b), which has been under debate for its partial attribution to the  
278 aerosol loading by the Australian Black Summer bushfire smoke injection into the stratosphere (e.g.,  
279 Santee et al. 2022; Solomon et al. 2023). While the magnitudes of the midlatitude ozone anomalies

280 were moderate, they were greater than 1 standard deviation estimated over the climatological period  
 281 of 1981-2018. The impact of the polar and mid-latitude zonal-mean ozone anomalies in 2020 on the  
 282 Antarctic circulation and temperature anomalies in the spring and summer of 2020-2021 will be  
 283 examined in the next section using forecast experiments testing the sensitivity to climatological vs.  
 284 realistic ozone forcing.



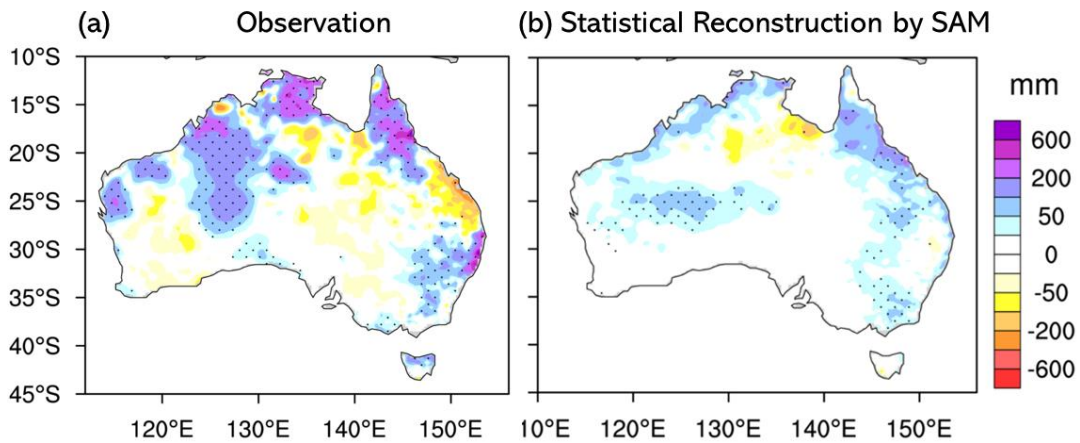
285

286 **Figure 5.** 2020 monthly mean anomalies of (a) zonal-mean zonal winds at 60°S, (b) the Antarctic polar cap  
 287 temperatures averaged over 60-90°S with cosine latitude weighting, and (c) zonal-mean zonal winds at 1 hPa.  
 288 Contours indicate the 1981-2018 climatologies with 10 ms<sup>-1</sup> and 10 K intervals for (a), (c) and (b), respectively.  
 289 Stippling indicates the magnitude of 2020 anomalies greater than 1σ estimated over the climatological period.  
 290 Wind and temperature data were de-trended before plotting, but de-trending did not make any significant  
 291 difference.



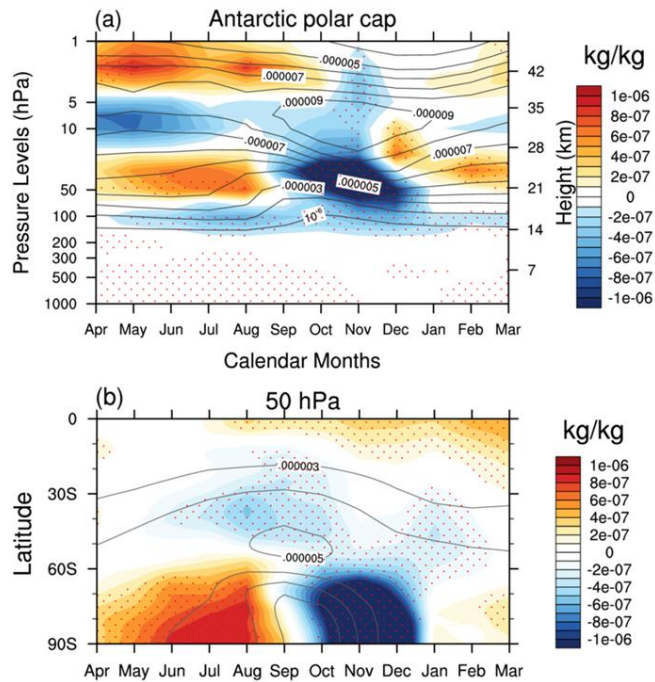
292

293 **Figure 6.** (a) Standardized amplitude of the SAM from April 2020 to March 2021 monitored by the NOAA Climate  
 294 Prediction Center Antarctic Oscillation index (CPC AAO; Thompson and Wallace 2000) and the British Antarctic  
 295 Survey's SAM index (BAS SAM; Marshall 2003). (b) Mean sea level pressure (MSLP) anomalies averaged over  
 296 the period from December 2020 to February 2021 (DJF 2020-21). Stippling indicates the magnitude of the 2020  
 297 anomalies greater than  $1\sigma$  estimated over the climatological period.



298

299 **Figure 7.** (a) DJF 2020-21 rainfall anomalies over Australia relative to the climatological mean of 1981-2018.  
 300 Stippling indicates the magnitude of the rainfall anomalies greater than  $1\sigma$  estimated over the climatological  
 301 period. (b) Reconstructed rainfall anomalies of DJF 2020-21 by regressing the DJF rainfall onto the CPC AAO  
 302 index for the period of 1981-2018 and scaling the resultant regression coefficient by the amplitude of the AAO  
 303 index in DJF 2020-21 ( $1.79\sigma$ ). Stippling indicates the statistical significance on the regression coefficients at the  
 304 90% confidence level, estimated by a two-sided student t-test, given 38 samples.



305

306 **Figure 8.** ERA5 ozone anomalies (a) over the Antarctic polar cap region of 60-90°S displayed as a function of  
 307 pressure level and calendar month and (b) in the lower stratosphere at 50 hPa displayed as a function of latitude  
 308 and calendar month. Contours indicate the 1981-2018 climatologies of the respective fields. In the calculation of  
 309 the climatologies, the ERA5 data for 2000-2006 were replaced by those of the ERA5.1 where lower stratosphere  
 310 cold biases and unrealistic spikes of ozone close to the South Pole in the winter months of 2003-2004 were fixed  
 311 (Simmons et al., 2020). Red-coloured stippling indicates the magnitude of the 2020 anomalies greater than 1 $\sigma$   
 312 estimated over the climatological period.

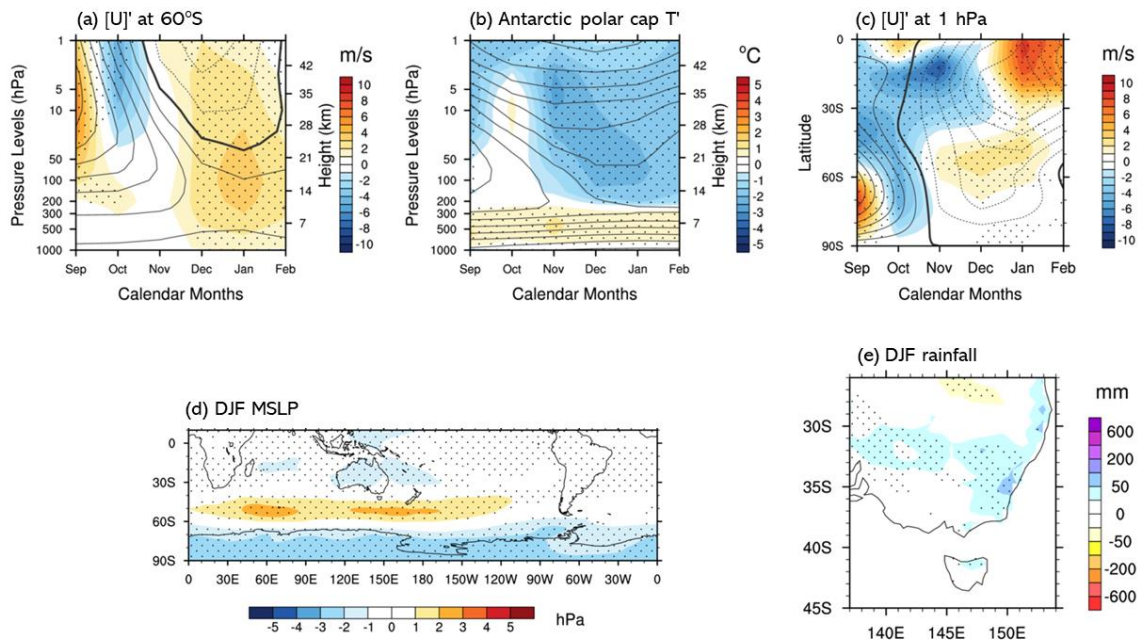
#### 313 4. ACCESS-S2 forecast experiments with two different ozone forcings

##### 314 4.1 Control forecasts with the climatological ozone forcing

315 ACCESS-S2 has statistically significant skill in predicting [U]' at 60°S and 10 hPa for the spring and  
 316 summer seasons in the hindcast period of 1990-2012 at up to 4-month lead time (Wedd et al. 2022).  
 317 For the October-December mean [U]' at 60°S and 10 hPa for the 1981-2018 climatological period  
 318 used in this study, the predictive skill of ACCESS-S2 is high with ~0.7 correlation at 1-month lead  
 319 time (i.e., forecasts initialized on 1 September and verified for the October-December mean) and  
 320 remains above the statistically significant level of 95% (> 0.33 correlation with 38 samples) at up to  
 321 3-month lead time (i.e., forecasts initialized on 1 July) (Fig. S3).

322 Despite the demonstrated hindcast skill, the 2020 strong vortex event of October-December was not  
 323 skilfully captured by the ensemble mean of ACCESS-S2 with the climatological ozone forcing  
 324 (control forecasts) at a relatively short lead time of 1 month (Fig. 9a). At this lead time, the model did  
 325 simulate an unusually cold polar stratosphere and unusually strong westerlies for late spring to  
 326 summer, but the predicted cooling was too mild and the stratospheric wind anomalies were delayed by  
 327 2 months compared to those in the reanalysis (Figs. 9a,b; cf., Figs 5a,b). The latitude-time evolution

328 of the upper stratospheric [U]' suggests that the forecast stratospheric winds followed the canonical  
 329 poleward evolution of the meridional dipole anomalies of the winter stratospheric jet (Fig. 9c), as  
 330 depicted by the regression pattern to the stratosphere-troposphere coupled mode index but with the  
 331 opposite sign (Fig. 3c). That is, the midlatitude easterly anomalies (flanked by high latitude westerly  
 332 anomalies) in the initial conditions of early September were forecast to migrate to the pole by October,  
 333 which did not happen in reality in 2020 (Fig. 5c).



334

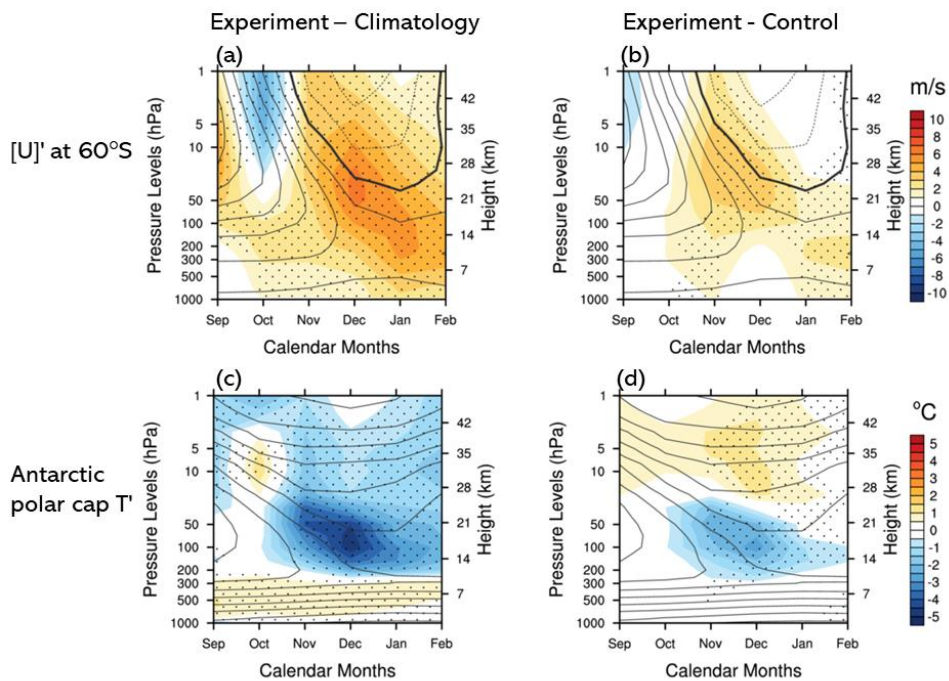
335 **Figure 9.** Control forecasts with the climatological ozone forcing for (a) [U]' at 60°S, (b) the Antarctic polar cap  
 336 averaged T', (c) [U]' at 1 hPa, (d) DJF mean MSLP anomalies, and (e) DJF mean rainfall anomalies of 2020-2021.  
 337 The contours in (a)-(c) indicate the ACCESS-S2 climatologies of the relevant fields computed over 1981-2018.  
 338 The contour interval is 10 ms<sup>-1</sup> in (a) and (c) and 10 K in (b). Stippling indicates the statistically significant  
 339 anomalies at the 90% confidence level as assessed by a two-tailed student t-test with 33 samples of the control  
 340 forecast set and 3 (ensemble members) x 38 (hindcast years) samples of the hindcast set.

341 In addition, the control forecasts predicted the maximum westerly anomalies in the troposphere rather  
 342 than in the stratosphere during summer (Fig. 9a; cf. Fig. 5a). Given that the observed westerly  
 343 anomalies also had a secondary maximum in the troposphere in February 2021 (Fig. 5a), the control  
 344 forecasts that missed the stratospheric westerly anomalies but hit the tropospheric westerly anomalies  
 345 may imply that the summer westerly anomalies could be in part driven by tropospheric processes,  
 346 possibly associated with La Niña (e.g., L'Heureux and Thompson 2006; Lim et al. 2016; Byrne et al.  
 347 2019). The good prediction of the westerly anomalies in DJF 2020-21 in the lower stratosphere and  
 348 the troposphere then skilfully led to the prediction of a positive SAM in that summer at 3-month lead  
 349 time despite the ozone forcing being climatological (Fig. 9d). The forecast also skilfully captured the  
 350 higher-than-normal rainfall over the eastern part of south-eastern Australia at 3-month lead time (Fig.  
 351 9e), which is likely due to the model's ability to predict the positive SAM and associated circulations

352 that bring rainfall to the region (Fig. S4). However, the positive rainfall was under-predicted. Also,  
 353 the wet forecast was extended too far to the west of the south-eastern region compared to the  
 354 observation, which seems partly due to the model bias in simulating the SAM and rainfall relationship  
 355 in the western area (Fig. S4).

#### 356 4.2 Experimental forecasts with the realistic ozone forcing of 2020-21

357 We presented in Figure 8 the lower-than-usual concentration of the Antarctic ozone observed in  
 358 spring 2020 in the lower stratosphere and the resultant lower-than-usual ozone concentration near the  
 359 Antarctic tropopause that persisted into the following autumn of 2021. When this low ozone was used  
 360 to force the ACCESS-S2 system, the Antarctic lower stratosphere was forecast to be substantially  
 361 colder during late spring and summer than that forced by the climatological ozone (Fig. 10 lower  
 362 panels) by reducing the ultraviolet radiation absorption and associated short-wave heating (e.g.,

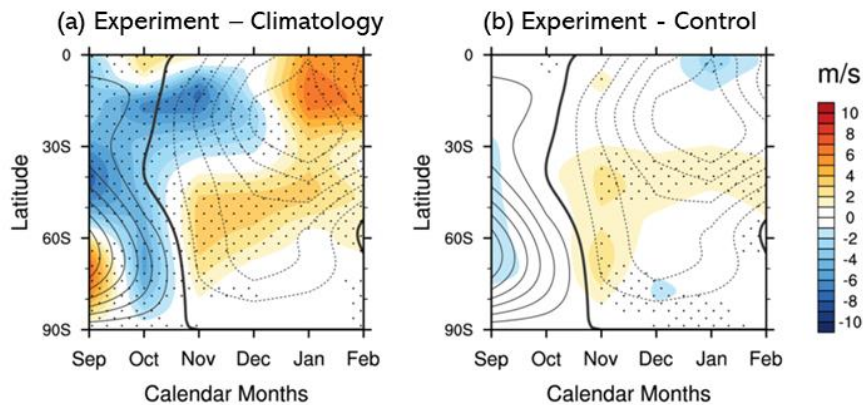


363

364 **Figure 10.** (Left panels) Experimental forecasts with the realistic ozone forcing of September 2020 – February  
 365 2021 for (a)  $[U]'$  at  $60^\circ\text{S}$  and (c) the Antarctic polar cap averaged  $T'$ . (Right panels) Differences made by the  
 366 realistic ozone forcing compared to the climatological ozone forcing for (b)  $[U]'$  at  $60^\circ\text{S}$  and (d) the Antarctic polar  
 367 cap averaged  $T'$ . In (a) and (c) the contours and stippling indicate the same as for Figure 9. In (b) and (d) the  
 368 contours indicate the hindcast climatologies of  $[U]'$  at  $60^\circ\text{S}$  and the Antarctic polar cap averaged  $T'$  as for Figure 9,  
 369 but the stippling denotes the statistically significant ensemble mean differences between the experimental and  
 370 control forecasts with 33 samples in each set.

371 Keeble et al. 2014). Consistent with this temperature change, the experimental forecasts simulated a  
 372 much stronger polar vortex during October to December 2020 in the stratosphere and stronger  
 373 westerlies during the following January to February in the lower stratosphere and troposphere than the

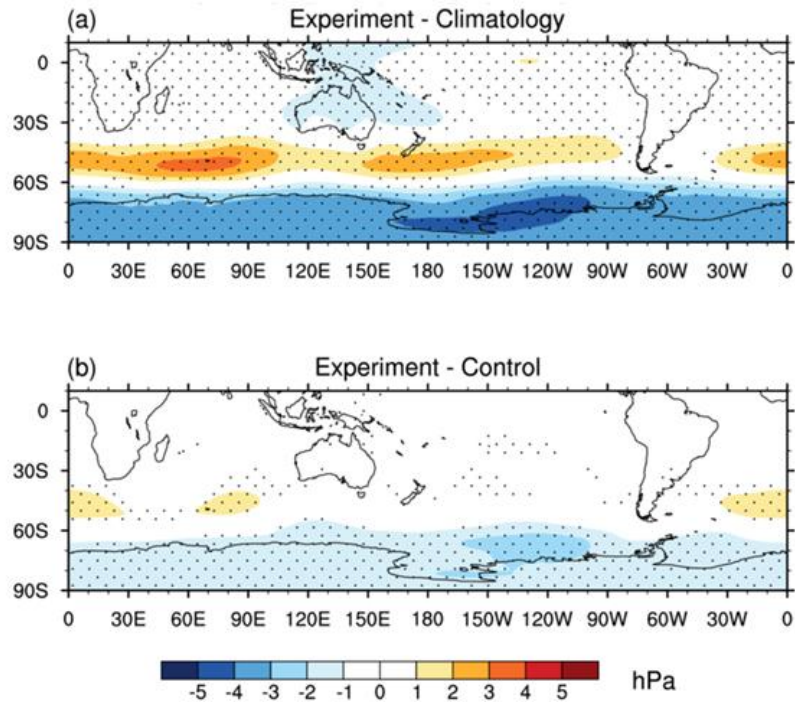
374 control forecasts (Fig. 10 upper panels), better matching the representation of the super vortex event  
 375 in the reanalysis (Fig. 5a). In addition, the impact of the realistic ozone forcing appears to have  
 376 reached the top of the stratosphere, making the forecast upper stratospheric zonal winds stronger in  
 377 November at 40-80°S (Fig. 11b), thereby delaying the vortex breakdown, which is similar to what  
 378 happened in 2020 (Fig. 5c).



379  
 380 **Figure 11.** The same as Figure 10 except [U] at 1 hPa.

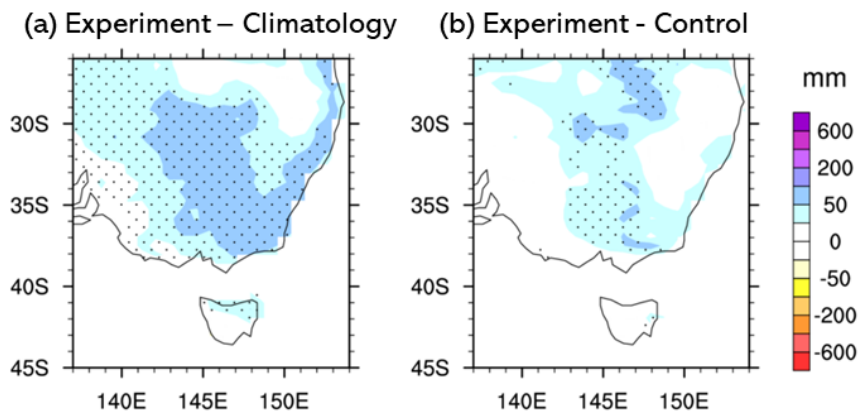
381 Since the forecast spring polar vortex and its downward coupling strengthened with the realistic ozone  
 382 forcing, a stronger positive SAM was predicted, especially with deeper low-pressure anomalies in the  
 383 Antarctic region (Fig. 12). A clear improvement in predicting the dipole pressure anomalies is also  
 384 seen in the southern Atlantic Ocean. Furthermore, the experimental forecasts with the 2020 ozone  
 385 generated substantially higher rainfall over south-eastern Australia than the control forecasts with the  
 386 climatological ozone, resulting in an improved forecast for the eastern part of south-eastern Australia  
 387 but a false alarm for above-average rainfall for the western part (Fig. 13a). Statistically significant  
 388 increases of rainfall generated by the realistic ozone forcing are found in the central part of south-  
 389 eastern Australia (Fig. 13b), which is more or less consistent with where the observed SAM and  
 390 rainfall relationship is prominent for 1981-2018 (Fig. 7b).

391 The improvements in predicting the polar stratospheric temperatures and vortex strength achieved by  
 392 the realistic ozone forcing are statistically significant at the 90% confidence level, and the  
 393 improvement in predicting the positive SAM in summer at the 3-month lead time is statistically  
 394 significant at the 95% confidence level, as assessed by a two-tailed paired student t-test with 33  
 395 forecast members in each set. The improvement in the south-eastern Australian summer rainfall  
 396 forecast at 3-month lead time is statistically significant at the 90% confidence level.



397

398 **Figure 12.** (a) Experimental forecasts with the realistic ozone forcing of 2020 for MSLP anomalies of DJF 2020-  
 399 21 when the forecasts were initialised on 1 September 2020. (b) Differences made by the realistic ozone forcing  
 400 compared to the climatological ozone forcing. The stippling indicates the statistical significance of the ensemble  
 401 mean difference (a) between the experimental forecasts and the 1981-2018 hindcasts and (b) between the  
 402 experimental forecasts and the control forecasts at the 90% confidence level, given 3x38 samples of the  
 403 hindcasts and 33 samples of the control and experimental forecasts as described in Figures 9 and 10.



404

405 **Figure 13.** The same as Figure 12 except rainfall anomalies of DJF 2020-21 over south-eastern Australia.

## 406 5. Concluding Remarks

407 In the last four years, the Antarctic stratosphere experienced exceptionally large variability, with a  
408 near-record/record-breaking stratospheric polar vortex weakening and warming event in spring 2019,  
409 followed by three persistently strong and cold polar vortex events in the spring seasons of 2020, 2021,  
410 and 2022. Among these cold events, the 2020 polar vortex, measured at 60°S and 10 hPa in October-  
411 December, was the strongest and coldest on record in the mid- to lower stratosphere for the late spring  
412 season since the beginning of the satellite observation in 1979. However, this super vortex event was  
413 not skilfully predicted by the BoM's dynamical S2S forecast system until the wind and temperature  
414 anomalies of the vortex were already substantially large. Motivated by this forecast challenge, we  
415 have explored the characteristics of the 2020 super vortex event and associated surface climate  
416 conditions; and attempted to understand a possible reason for the lack of long-lead predictability of  
417 this vortex event and a potential role of realistic ozone forcing for the vortex strength and evolution  
418 and its downward coupling. We have tackled these research problems by conducting forecast  
419 sensitivity experiments to the climatological ozone vs. the realistic 2020 ozone forcing, having  
420 considered that realistic ozone forcing is missing in the BoM's dynamical S2S forecast systems,  
421 ACCESS-S1/S2.

422 Our results have shown that the 2020 super vortex event did not follow the usual linear dynamical  
423 processes, which involve wave-mean flow feedback and associated poleward transition of dipole  
424 anomalies of the winter stratospheric jet at the top of the stratosphere. In fact, the poleward shift of the  
425 jet and increased upward propagating wave activities in the SH extratropics in winter were suggestive  
426 of a polar vortex weakening and warming event in spring 2020. Although the occurrence of this  
427 strong vortex event was unexpected, its downward coupling was typical for such an event, resulting in  
428 a positive SAM at the surface in the following summer, which is likely to have promoted increased  
429 summer rainfall over the eastern part of south-eastern Australia.

430 The ACCESS-S2 33-member ensemble mean forecasts forced with the climatological ozone (control  
431 forecasts) fell short in predicting the stronger-than-normal October-December mean vortex measured  
432 at 60°S and 10 hPa at 1-month lead time. This was because the model simulated a poleward shift of  
433 the jet with the midlatitude easterly anomalies present at the beginning of September, which did not  
434 occur in reality. However, the control forecasts eventually simulated stronger-than-normal westerlies  
435 in the lower stratosphere to the troposphere in summer and a delayed vortex breakdown in the upper  
436 stratosphere, consistent with those represented in the reanalyses. Consequently, the positive SAM in  
437 the summer of 2020-21 was skilfully predicted even with the climatological ozone forcing. The  
438 experimental set of 33-member ensemble mean forecasts forced with the ERA-5 ozone of 2020 more  
439 skilfully simulated the unusually cold polar stratosphere and the unusually strong and persistent

440 vortex in the spring and early summer of 2020, which led to better predictions of the positive SAM in  
441 the summer and associated wetter-than-normal conditions over the east of south-eastern Australia.

442 Overall, these findings on the role of ozone in the predictability of the tropospheric SAM and  
443 associated Australian rainfall are consistent with the results shown in previous studies (Thompson et  
444 al. 2005; Fogt et al. 2009; Kang et al. 2011; Son et al. 2013; Hendon et al. 2020; Oh et al. 2022). Our  
445 study reveals that ozone also plays an important role in shaping the temporal evolution of polar  
446 stratospheric temperature anomalies, and that the impact of using realistic ozone is not limited to the  
447 lower stratosphere where the ozone anomalies are concentrated but can reach into the upper  
448 stratosphere, therefore influencing the timing of the vortex breakdown. These novel results highlight  
449 the importance of ozone as a source of predictability yet to be exploited for S2S forecasts. Thus, we  
450 argue that future model development efforts should prioritise improving representations of ozone  
451 forcing for seasonal prediction systems through a novel parameterisation scheme or an affordable  
452 interactive chemistry scheme. On this note, it is worth mentioning a caveat that our forecast sensitivity  
453 experiments to prescribed climatological *vs.* observed ozone forcing demonstrate the predictability  
454 explained by the perfect knowledge of zonal-mean ozone; but if an interactive chemistry scheme is  
455 implemented in dynamical forecast systems, predictions of ozone would be linked to other forecast  
456 variables such as winds and temperatures and subsequent feedbacks. Therefore, in such a case, the  
457 maximum benefit of improving ozone forcing in dynamical forecasts will only be realised when  
458 forecast skill for the dynamics associated with the polar vortex and its downward coupling is reliably  
459 high.

460 Although we diagnosed the atypical evolution of the 2020 super vortex, which was not skilfully  
461 captured by the ACCESS-S2 system at 1-month lead time, a future study is needed to understand why  
462 the sudden development occurred; this will require in-depth investigation of the middle atmospheric  
463 dynamics in 2020. Another interesting subject to explore may be a possible contribution of La Niña to  
464 the different stages of the 2020 vortex life cycle and the surface SAM (Byrne et al. 2019), given the  
465 frequent concurrence of La Niña and unusually strong Antarctic stratospheric vortex events (e.g., in  
466 1998-99, 2010-11 and 2020-2022) even though previous work did not show a significant linear  
467 relationship between canonical eastern Pacific-type El Niño and Antarctic stratospheric vortex  
468 variability (e.g., Hurwitz et al. 2011; Lim et al. 2018).

## 469 Acknowledgements

470 This study is part of the Victorian Water and Climate Initiative (VicWaCI), funded by the Department  
471 of the Energy, Environment, and Climate Action; the National Environmental Science Program  
472 (NESP), funded by the Department of Climate Change, Energy, the Environment and Water; and the  
473 Australian Research Council Special Research Initiative for Securing Antarctica's Environmental  
474 Future (SAEF) Program (SR200100005). S. A. acknowledges the Australian Research Council's  
475 Discovery Project (DP220101468). J. M. A. was partially supported by the Regional and Global  
476 Model Analysis component of the Earth and Environmental System Modeling Program of the U.S.  
477 Department of Energy's Office of Biological and Environmental Research via National Science  
478 Foundation IA 1947282. S.-W. S. was supported by the Korea Environment Industry & Technology  
479 Institute (KEITI) through "Climate Change R&D Project for New Climate Regime.", funded by the  
480 Korea Ministry of Environment (MOE) (2022003560004). G. L. Manney was supported by the Jet  
481 Propulsion Laboratory (JPL) Microwave Limb Sounder team under JPL subcontract #1521127 to  
482 NWRA, and by NSF Climate and Large-scale Dynamics Grant #2015906. This research was  
483 undertaken on the NCI National Facility in Canberra, Australia, which is supported by the Australian  
484 Commonwealth Government. The authors thank Ms Jo Croucher and Drs Yiling Liu and Heather  
485 Leasor at the NCI for their great efforts to make the BoM forecast data publicly available on the NCI  
486 data server. The NCAR Command Language (NCL; <http://www.ncl.ucar.edu>) version and Python  
487 version 2.7.16 were used for data analysis and visualization of the results. We acknowledge the  
488 Japanese Meteorological Agency, NCAR/UCAR, ECMWF, and BoM for producing/archiving the  
489 JRA-55 reanalysis, the ERA5 reanalysis, and the Australian gridded climate data, respectively. We  
490 also acknowledge the NOAA CPC, the British Antarctic Survey, and the NASA for the availability of  
491 the Antarctic Oscillation index, an observation-based SAM index, and the Antarctic total column  
492 ozone data, respectively. The authors want to thank Drs. Debra Hudson and Ghyslaine Boschat at the  
493 BoM for their valuable and constructive feedback on the manuscript.

## 494 Open Research

### 495 Data Availability Statement

496 The JRA-55 monthly mean reanalysis set is available at [NCAR Research Data Archive \(ucar.edu\)](https://www.ncl.ucar.edu).  
497 The ERA5 monthly ozone reanalysis data are available at  
498 [https://cds.climate.copernicus.eu/cdsapp#!/dataset/reanalysis-era5-single-levels-monthly-](https://cds.climate.copernicus.eu/cdsapp#!/dataset/reanalysis-era5-single-levels-monthly-means?tab=overview)  
499 [means?tab=overview](https://cds.climate.copernicus.eu/cdsapp#!/dataset/reanalysis-era5-single-levels-monthly-means?tab=overview). The Antarctic Oscillation Index is available at  
500 [https://www.cpc.ncep.noaa.gov/products/precip/CWlink/daily\\_ao\\_index/aao/aao.shtml](https://www.cpc.ncep.noaa.gov/products/precip/CWlink/daily_ao_index/aao/aao.shtml). Marshall  
501 (2003)'s observation-based SAM index is available at <http://www.nerc-bas.ac.uk/icd/gjma/sam.html>.  
502 The Antarctic total column ozone data are from the NASA Ozone Watch  
503 (<https://ozonewatch.gsfc.nasa.gov/SH.html>). The Australian gridded climate data are available at

504 <http://www.bom.gov.au/climate/data/>. The BoM hindcast and control and experimental forecast data  
505 are available at <https://doi.org/10.25914/8fdt-6v74>. The NCL software resources are available at  
506 <https://www.ncl.ucar.edu/>.

## 507 References

508 Andrews, D. G., Holton, J. R., & Leovy, C. B. (1987). *Middle Atmosphere Dynamics*. Academic Press,  
509 Inc.

510 Baldwin, M. P., Ayarzagüena, B., Birner, T., Butchart, N., Butler, A. H., Charlton-Perez, A. J.,  
511 Domeisen, D. I. V., Garfinkel, C. I., Garny, H., Gerber, E. P., Hegglin, M. I., Langematz, U., &  
512 Pedatella, N. M. (2021). Sudden Stratospheric Warmings. *Reviews of Geophysics*, 59(1).  
513 <https://doi.org/10.1029/2020RG000708>

514 Black, R. X., & McDaniel, B. A. (2007). Interannual Variability in the Southern Hemisphere  
515 Circulation Organized by Stratospheric Final Warming Events. *Journal of the Atmospheric*  
516 *Sciences*, 64(8), 2968–2974. <https://doi.org/10.1175/JAS3979.1>

517 Bureau of Meteorology. (2019). APS3 upgrade of the ACCESS-G/GE Numerical Weather Prediction  
518 System. *National Operational Centre Operations Bulletin Number 125*.

519 Byrne, N. J., & Shepherd, T. G. (2018). Seasonal Persistence of Circulation Anomalies in the  
520 Southern Hemisphere Stratosphere and Its Implications for the Troposphere. *Journal of Climate*,  
521 31(9), 3467–3483. <https://doi.org/10.1175/JCLI-D-17-0557.1>

522 Byrne, N. J., Shepherd, T. G., & Polichtchouk, I. (2019). Subseasonal-to-Seasonal Predictability of  
523 the Southern Hemisphere Eddy-Driven Jet During Austral Spring and Early Summer. *Journal of*  
524 *Geophysical Research: Atmospheres*, 124(13), 2018JD030173.  
525 <https://doi.org/10.1029/2018JD030173>

526 Cionni, I., Eyring, V., Lamarque, J. F., Randel, W. J., Stevenson, D. S., Wu, F., Bodeker, G. E.,  
527 Shepherd, T. G., Shindell, D. T., & Waugh, D. W. (2011). Ozone database in support of CMIP5  
528 simulations: results and corresponding radiative forcing. *Atmospheric Chemistry and Physics*,  
529 11(21), 11267–11292. <https://doi.org/10.5194/acp-11-11267-2011>

530 Dee, D. P., Uppala, S. M., Simmons, A. J., Berrisford, P., Poli, P., Kobayashi, S., Andrae, U.,  
531 Balmaseda, M. A., Balsamo, G., Bauer, P., Bechtold, P., Beljaars, A. C. M., van de Berg, L.,  
532 Bidlot, J., Bormann, N., Delsol, C., Dragani, R., Fuentes, M., Geer, A. J., ... Vitart, F. (2011).  
533 The ERA-Interim reanalysis: configuration and performance of the data assimilation system.  
534 *Quarterly Journal of the Royal Meteorological Society*, 137(656), 553–597.  
535 <https://doi.org/10.1002/qj.828>

- 536 Evans, A., Jones, D., Smalley, R., & Lellyett, S. (2020). An enhanced gridded rainfall dataset scheme  
537 for Australia. In *Bureau Research Report No. 41* (Issue June).  
538 [https://www.google.com.au/search?q=An+enhanced+gridded+rainfall+analysis+scheme+for+Australia&rls=com.microsoft%3Aen-](https://www.google.com.au/search?q=An+enhanced+gridded+rainfall+analysis+scheme+for+Australia&rls=com.microsoft%3Aen-GB%3A%7Breferrer%3Asource%7D&sxsrf=ALiCzsbui9q6NgSQW0jYNPHo_q7dSMvDnQ%3A1662425730786&ei=gpoWY9PVL4SdseMPjuym4A0&ved=0ahUKEwjTnpi5-v75AhWE)  
539 [GB%3A%7Breferrer%3Asource%7D&sxsrf=ALiCzsbui9q6NgSQW0jYNPHo\\_q7dSMvDnQ%3A1662425730786&ei=gpoWY9PVL4SdseMPjuym4A0&ved=0ahUKEwjTnpi5-v75AhWE](https://www.google.com.au/search?q=An+enhanced+gridded+rainfall+analysis+scheme+for+Australia&rls=com.microsoft%3Aen-GB%3A%7Breferrer%3Asource%7D&sxsrf=ALiCzsbui9q6NgSQW0jYNPHo_q7dSMvDnQ%3A1662425730786&ei=gpoWY9PVL4SdseMPjuym4A0&ved=0ahUKEwjTnpi5-v75AhWE)
- 542 Fogt, R. L., & Marshall, G. J. (2020). The Southern Annular Mode: Variability, trends, and climate  
543 impacts across the Southern Hemisphere. *Wiley Interdisciplinary Reviews: Climate Change*,  
544 *11*(4), 1–24. <https://doi.org/10.1002/wcc.652>
- 545 Fogt, R. L., Perlwitz, J., Pawson, S., & Olsen, M. A. (2009). Intra-annual relationships between polar  
546 ozone and the SAM. *Geophysical Research Letters*, *36*(4), 1–6.  
547 <https://doi.org/10.1029/2008GL036627>
- 548 Friedel, M., Chiodo, G., Stenke, A., Domeisen, D. I. V., Fueglistaler, S., Anet, J. G., & Peter, T.  
549 (2022). Springtime arctic ozone depletion forces northern hemisphere climate anomalies. *Nature*  
550 *Geoscience*, *15*(7), 541–547. <https://doi.org/10.1038/s41561-022-00974-7>
- 551 Gillett, N. P., Kell, T. D., & Jones, P. D. (2006). Regional climate impacts of the Southern Annular  
552 Mode. *Geophysical Research Letters*, *33*(23), L23704. <https://doi.org/10.1029/2006GL027721>
- 553 Gong, D., & Wang, S. (1999). Definition of Antarctic Oscillation index. *Geophysical Research*  
554 *Letters*, *26*(4), 459–462. <https://doi.org/10.1029/1999GL900003>
- 555 Hartmann, D. L. (2022). The Antarctic ozone hole and the pattern effect on climate sensitivity.  
556 *Proceedings of the National Academy of Sciences of the United States of America*, *119*(35), 1–5.  
557 <https://doi.org/10.1073/pnas.2207889119>
- 558 Hartmann, D. L., Mechoso, C. R., & Yamazaki, K. (1984). Observations of Wave-Mean Flow  
559 Interaction in the Southern Hemisphere. In *Journal of Atmospheric Sciences* (Vol. 41, Issue 3,  
560 pp. 351–362). [https://doi.org/10.1175/1520-0469\(1984\)041<0351:OOWMFI>2.0.CO;2](https://doi.org/10.1175/1520-0469(1984)041<0351:OOWMFI>2.0.CO;2)
- 561 Heidemann, H., Cowan, T., Henley, B. J., Ribbe, J., Freund, M., & Power, S. (2023). Variability and  
562 long-term change in Australian monsoon rainfall: A review. *Wiley Interdisciplinary Reviews:*  
563 *Climate Change, January 2022*, 1–28. <https://doi.org/10.1002/wcc.823>
- 564 Hendon, H. H., Lim, E.-P., Arblaster, J. M., & Anderson, D. L. T. (2014). Causes and predictability of  
565 the record wet east Australian spring 2010. *Climate Dynamics*, *42*(5–6), 1155–1174.  
566 <https://doi.org/10.1007/s00382-013-1700-5>
- 567 Hendon, H. H., Lim, E. -P., & Abhik, S. (2020). Impact of Interannual Ozone Variations on the

568 Downward Coupling of the 2002 Southern Hemisphere Stratospheric Warming. *Journal of*  
569 *Geophysical Research: Atmospheres*, October 2002, 1–16.  
570 <https://doi.org/10.1029/2020JD032952>

571 Hendon, H. H., Thompson, D. W. J., & Wheeler, M. C. (2007). Australian rainfall and surface  
572 temperature variations associated with the Southern Hemisphere annular mode. *Journal of*  
573 *Climate*, 20(11), 2452–2467. <https://doi.org/10.1175/JCLI4134.1>

574 Henley, B. J., Gergis, J., Karoly, D. J., Power, S., Kennedy, J., & Folland, C. K. (2015). A Tripole  
575 Index for the Interdecadal Pacific Oscillation. *Climate Dynamics*, 45(11–12), 3077–3090.  
576 <https://doi.org/10.1007/s00382-015-2525-1>

577 Hersbach, H., Bell, B., Berrisford, P., Hirahara, S., Horányi, A., Muñoz-Sabater, J., Nicolas, J.,  
578 Peubey, C., Radu, R., Schepers, D., Simmons, A., Soci, C., Abdalla, S., Abellan, X., Balsamo,  
579 G., Bechtold, P., Biavati, G., Bidlot, J., Bonavita, M., ... Thépaut, J. N. (2020). The ERA5  
580 global reanalysis. *Quarterly Journal of the Royal Meteorological Society*, 146(730), 1999–2049.  
581 <https://doi.org/10.1002/qj.3803>

582 Hio, Y., & Yoden, S. (2004). Quasi-Periodic Variations of the Polar Vortex in the Southern  
583 Hemisphere Stratosphere Due to Wave–Wave Interaction. *Journal of the Atmospheric Sciences*,  
584 61(21), 2510–2527. <https://doi.org/10.1175/JAS3257.1>

585 Hio, Y., & Yoden, S. (2005). Interannual Variations of the Seasonal March in the Southern  
586 Hemisphere Stratosphere for 1979–2002 and Characterization of the Unprecedented Year 2002.  
587 *Journal of the Atmospheric Sciences*, 62(3), 567–580. <https://doi.org/10.1175/JAS-3333.1>

588 Hudson et. al., D. (2017). ACCESS-S1 The new Bureau of Meteorology multi-week to seasonal  
589 prediction system. *Journal of Southern Hemisphere Earth System Science*, 67(3), 132–159.  
590 <https://doi.org/10.22499/3.6703.001>

591 Hurwitz, M. M., Newman, P. A., Oman, L. D., & Molod, A. M. (2011). Response of the Antarctic  
592 Stratosphere to Two Types of El Niño Events. *Journal of the Atmospheric Sciences*, 68(4), 812–  
593 822. <https://doi.org/10.1175/2011JAS3606.1>

594 Jones, D. A., Wang, W., & Fawcett, R. (2009). High-quality spatial climate data-sets for Australia.  
595 *Australian Meteorological and Oceanographic Journal*, 58, 233–248.

596 Kang, S. M., Polvani, L. M., Fyfe, J. C., & Sigmond, M. (2011). Impact of polar ozone depletion on  
597 subtropical precipitation. *Science*, 332(2011), 951–954. <https://doi.org/10.1126/science.1202131>

598 Keeble, J., Braesicke, P., Abraham, N. L., Roscoe, H. K., & Pyle, J. A. (2014). The impact of polar  
599 stratospheric ozone loss on southern Hemisphere stratospheric circulation and climate.

600 *Atmospheric Chemistry and Physics*, 14(24), 13705–13717. <https://doi.org/10.5194/acp-14->  
601 13705-2014

602 Kidson, J. W. (1988). Indices of the Southern Hemisphere Zonal Wind. In *Journal of Climate* (Vol. 1,  
603 Issue 2, pp. 183–194). [https://doi.org/10.1175/1520-0442\(1988\)001<0183:IOTSHZ>2.0.CO;2](https://doi.org/10.1175/1520-0442(1988)001<0183:IOTSHZ>2.0.CO;2)

604 Kobayashi, S., Ota, Y., Harada, Y., Ebata, A., Moriya, M., Onoda, H., Onogi, K., Kamahori, H.,  
605 Kobayashi, C., Endo, H., Miyaoka, K., & Takahashi, K. (2015). The JRA-55 Reanalysis:  
606 General Specifications and Basic Characteristics. *Journal of the Meteorological Society of Japan*.  
607 *Ser. II*, 93(1), 5–48. <https://doi.org/10.2151/jmsj.2015-001>

608 Kosaka, Y., & Xie, S.-P. (2013). Recent global-warming hiatus tied to equatorial Pacific surface  
609 cooling. *Nature*, 501(7467), 403–407. <https://doi.org/10.1038/nature12534>

610 Kuroda, Y., & Kodera, K. (1998). Interannual variability in the troposphere and stratosphere of the  
611 Southern Hemisphere winter. *Journal of Geophysical Research: Atmospheres*, 103(D12),  
612 13787–13799. <https://doi.org/10.1029/98JD01042>

613 L’Heureux, M. L., & Thompson, D. W. J. (2006). Observed relationships between the El Niño–  
614 Southern Oscillation and the extratropical zonal-mean circulation. *Journal of Climate*, 19(2),  
615 276–287. <https://doi.org/10.1175/JCLI3617.1>

616 Levelt, P. F., van den Oord, G. H. J., Dobber, M. R., Malkki, A., Huib Visser, Johan de Vries,  
617 Stammes, P., Lundell, J. O. V., & Saari, H. (2006). The ozone monitoring instrument. *IEEE*  
618 *Transactions on Geoscience and Remote Sensing*, 44(5), 1093–1101.  
619 <https://doi.org/10.1109/TGRS.2006.872333>

620 Lim, E.-P., & Hendon, H. H. (2015). Understanding and predicting the strong Southern Annular  
621 Mode and its impact on the record wet east Australian spring 2010. *Climate Dynamics*, 44(9–10),  
622 2807–2824. <https://doi.org/10.1007/s00382-014-2400-5>

623 Lim, E.-P., Hendon, H. H., Arblaster, J. M., Chung, C., Moise, A. F., Hope, P., Young, G., & Zhao, M.  
624 (2016). Interaction of the recent 50 year SST trend and La Niña 2010: amplification of the  
625 Southern Annular Mode and Australian springtime rainfall. *Climate Dynamics*, 47(7–8), 2273–  
626 2291. <https://doi.org/10.1007/s00382-015-2963-9>

627 Lim, E.-P., Hendon, H. H., Boschhat, G., Hudson, D., Thompson, D. W. J., Dowdy, A. J., & Arblaster,  
628 J. M. (2019). Australian hot and dry extremes induced by weakenings of the stratospheric polar  
629 vortex. *Nature Geoscience*, 12(11), 896–901. <https://doi.org/10.1038/s41561-019-0456-x>

630 Lim, E.-P., Hendon, H. H., & Thompson, D. W. J. (2018). Seasonal evolution of stratosphere–  
631 troposphere coupling in the Southern Hemisphere and implications for the predictability of

632 surface climate. *Journal of Geophysical Research: Atmospheres*, 123, 12,002–12,016.  
633 <https://doi.org/10.1029/2018JD029321>

634 Lim, E. P., Hendon, H. H., Butler, A. H., Thompson, D. W. J., Lawrence, Z. D., Scaife, A. A.,  
635 Shepherd, T. G., Polichtchouk, I., Nakamura, H., Kobayashi, C., Comer, R., Coy, L., Dowdy, A.,  
636 Garreaud, R. D., Newman, P. A., & Wang, G. (2021). Supplementary Material - The 2019  
637 southern hemisphere stratospheric polar vortex weakening and its impacts. *Bulletin of the*  
638 *American Meteorological Society*, 102(6), E1150–E1171. [https://doi.org/10.1175/BAMS-D-20-](https://doi.org/10.1175/BAMS-D-20-0112.1)  
639 0112.1

640 Limpasuvan, V., Hartmann, D. L., Thompson, D. W. J., Jeev, K., & Yung, Y. L. (2005). Stratosphere-  
641 troposphere evolution during polar vortex intensification. *Journal of Geophysical Research*,  
642 110(D24), D24101. <https://doi.org/10.1029/2005JD006302>

643 MacLachlan, C., Arribas, A., Peterson, K. A., Maidens, A., Fereday, D., Scaife, A. A., Gordon, M.,  
644 Vellinga, M., Williams, A., Comer, R. E., Camp, J., Xavier, P., & Madec, G. (2015). Global  
645 Seasonal forecast system version 5 (GloSea5): a high-resolution seasonal forecast system.  
646 *Quarterly Journal of the Royal Meteorological Society*, 141(689), 1072–1084.  
647 <https://doi.org/10.1002/qj.2396>

648 Marshall, G. J. (2003). Trends in the Southern Annular Mode from observations and reanalyses.  
649 *Journal of Climate*, 16(24), 4134–4143. [https://doi.org/10.1175/1520-](https://doi.org/10.1175/1520-0442(2003)016<4134:TITSAM>2.0.CO;2)  
650 0442(2003)016<4134:TITSAM>2.0.CO;2

651 Matsuno, T. (1970). Vertical Propagation of Stationary Planetary Waves in the Winter Northern  
652 Hemisphere. *Journal of the Atmospheric Sciences*, 27(6), 871–883.  
653 [https://doi.org/10.1175/1520-0469\(1970\)027<0871:VPOSPW>2.0.CO;2](https://doi.org/10.1175/1520-0469(1970)027<0871:VPOSPW>2.0.CO;2)

654 McBride, J. L., & Nicholls, N. (1983). Seasonal Relationships between Australian Rainfall and the  
655 Southern Oscillation. *Monthly Weather Review*, 111(10), 1998–2004.  
656 [https://doi.org/10.1175/1520-0493\(1983\)111<1998:SRBARA>2.0.CO;2](https://doi.org/10.1175/1520-0493(1983)111<1998:SRBARA>2.0.CO;2)

657 Noguchi, S., Kuroda, Y., Kodera, K., & Watanabe, S. (2020). Robust Enhancement of Tropical  
658 Convective Activity by the 2019 Antarctic Sudden Stratospheric Warming. *Geophysical*  
659 *Research Letters*, 47(15). <https://doi.org/10.1029/2020GL088743>

660 North, G. R., Bell, T. L., Cahalan, R. F., & Moeng, F. J. (1982). Sampling Errors in the Estimation of  
661 Empirical Orthogonal Functions. *Monthly Weather Review*, 110(7), 699–706.  
662 [https://doi.org/10.1175/1520-0493\(1982\)110<0699:seiteo>2.0.co;2](https://doi.org/10.1175/1520-0493(1982)110<0699:seiteo>2.0.co;2)

663 Oh, J., Son, S. W., Choi, J., Lim, E. P., Garfinkel, C., Hendon, H., & Kim, Y. (2022). Impact of  
664 stratospheric ozone on the subseasonal prediction in the southern hemisphere spring. *Progress in*

665 *Earth and Planetary Science*. <https://doi.org/10.1186/s40645-022-00485-4>

666 Polvani, L. M., & Waugh, D. W. (2004). Upward wave activity flux as a precursor to extreme  
667 stratospheric events and subsequent anomalous surface weather regimes. *Journal of Climate*,  
668 17(18), 3548–3554. [https://doi.org/10.1175/1520-0442\(2004\)017<3548:UWAFAA>2.0.CO;2](https://doi.org/10.1175/1520-0442(2004)017<3548:UWAFAA>2.0.CO;2)

669 Randel, W. J., & Newman, P. A. (1998). The Stratosphere in the Southern Hemisphere. In  
670 *Meteorology of the Southern Hemisphere* (pp. 243–282). American Meteorological Society.  
671 [https://doi.org/10.1007/978-1-935704-10-2\\_9](https://doi.org/10.1007/978-1-935704-10-2_9)

672 Rao, J., Garfinkel, C. I., White, I. P., & Schwartz, C. (2020). The Southern Hemisphere Minor Sudden  
673 Stratospheric Warming in September 2019 and its Predictions in S2S Models. *Journal of*  
674 *Geophysical Research: Atmospheres*, 125(14), 1–19. <https://doi.org/10.1029/2020JD032723>

675 Reason, C. J. C., & Rouault, M. (2005). Links between the Antarctic Oscillation and winter rainfall  
676 over western South Africa. *Geophysical Research Letters*, 32(7), 1–4.  
677 <https://doi.org/10.1029/2005GL022419>

678 Rieger, L. A., Randel, W. J., Bourassa, A. E., & Solomon, S. (2021). Stratospheric Temperature and  
679 Ozone Anomalies Associated With the 2020 Australian New Year Fires. *Geophysical Research*  
680 *Letters*, 48(24), 1–8. <https://doi.org/10.1029/2021GL095898>

681 Risbey, J. S., Pook, M. J., McIntosh, P. C., Wheeler, M. C., & Hendon, H. H. (2009). On the remote  
682 drivers of rainfall variability in Australia. *Monthly Weather Review*, 137(10), 3233–3253.  
683 <https://doi.org/10.1175/2009MWR2861.1>

684 Salby, M., Titova, E., & Deschamps, L. (2011). Rebound of antarctic ozone. *Geophysical Research*  
685 *Letters*, 38(9), 2–5. <https://doi.org/10.1029/2011GL047266>

686 Santee, M. L., Lambert, A., Manney, G. L., Livesey, N. J., Froidevaux, L., Neu, J. L., Schwartz, M. J.,  
687 Millán, L. F., Werner, F., Read, W. G., Park, M., Fuller, R. A., & Ward, B. M. (2022).  
688 Prolonged and Pervasive Perturbations in the Composition of the Southern Hemisphere  
689 Midlatitude Lower Stratosphere From the Australian New Year’s Fires. *Geophysical Research*  
690 *Letters*, 49(4), 1–11. <https://doi.org/10.1029/2021GL096270>

691 Sen Gupta, A., & England, M. H. (2006). Coupled ocean-atmosphere-ice response to variations in the  
692 southern annular mode. *Journal of Climate*, 19(18), 4457–4486.  
693 <https://doi.org/10.1175/JCLI3843.1>

694 Seviour, W. J. M., Hardiman, S. C., Gray, L. J., Butchart, N., MacLachlan, C., & Scaife, A. A. (2014).  
695 Skillful seasonal prediction of the Southern Annular Mode and Antarctic ozone. *Journal of*  
696 *Climate*, 27(19), 7462–7474. <https://doi.org/10.1175/JCLI-D-14-00264.1>

- 697 Sharmila, S., & Hendon, H. H. (2020). Mechanisms of multiyear variations of Northern Australia wet-  
698 season rainfall. *Scientific Reports*, *10*(1), 1–11. <https://doi.org/10.1038/s41598-020-61482-5>
- 699 Shaw, T. A., Perlwitz, J., & Harnik, N. (2010). Downward wave coupling between the stratosphere  
700 and troposphere: The importance of meridional wave guiding and comparison with zonal-mean  
701 coupling. *Journal of Climate*, *23*(23), 6365–6381. <https://doi.org/10.1175/2010JCLI3804.1>
- 702 Shen, X., Wang, L., & Osprey, S. (2020). Tropospheric Forcing of the 2019 Antarctic Sudden  
703 Stratospheric Warming. *Geophysical Research Letters*, *47*(20), 1–8.  
704 <https://doi.org/10.1029/2020GL089343>
- 705 Shen, X., Wang, L., Osprey, S., Hardiman, S. C., Scaife, A. A., & Ma, A. J. I. (2022). The Life Cycle  
706 and Variability of Antarctic Weak Polar Vortex Events. *Journal of Climate*, *35*(6), 2075–2092.  
707 <https://doi.org/10.1175/JCLI-D-21-0500.1>
- 708 Shiotani, M., Shimoda, N., & Hirota, I. (1993). Interannual variability of the stratospheric circulation  
709 in the Southern Hemisphere. *Quarterly Journal of the Royal Meteorological Society*, *119*(511),  
710 531–546.
- 711 Silvestri, G. E., & Vera, C. S. (2003). Antarctic Oscillation signal on precipitation anomalies over  
712 southeastern South America. *Geophysical Research Letters*, *30*(21), 2115.  
713 <https://doi.org/10.1029/2003GL018277>
- 714 Simmons, A., Soci, C., Nicolas, J., Bell, B., Berrisford, P., Dragani, R., Flemming, J., Haimberger, L.,  
715 Healy, S., & Hersbach, H. (2020). *Technical Memo ECMWF. January.*
- 716 Solomon, S., Ivy, D. J., Kinnison, D., Mills, M. J., Iii, R. R. N., & Schmidt, A. (2016). *Emergence of*  
717 *healing in the Antarctic ozone layer. 0061.*
- 718 Solomon, S., Stone, K., Yu, P., Murphy, D. M., Kinnison, D., Ravishankara, A. R., & Wang, P.  
719 (2023). Chlorine activation and enhanced ozone depletion induced by wildfire aerosol. *Nature*,  
720 *615*(7951), 259–264. <https://doi.org/10.1038/s41586-022-05683-0>
- 721 Son, S. W., Purich, A., Hendon, H. H., Kim, B. M., & Polvani, L. M. (2013). Improved seasonal  
722 forecast using ozone hole variability? Supplementary Info. *Geophysical Research Letters*,  
723 *40*(23), 6231–6235. <https://doi.org/10.1002/2013GL057731>
- 724 SPARC. (2022). SPARC Reanalysis Intercomparison Project (S-RIP) Final Report. In M. Fujiwara, G.  
725 L. Manney, L. J. Gray, & J. S. Wright (Eds.), *SPARC Report No. 10/WCRP Report 6/2021.*  
726 <https://doi.org/10.17874/800dee57d13>
- 727 Stammerjohn, S. E., Martinson, D. G., Smith, R. C., Yuan, X., & Rind, D. (2008). Trends in Antarctic  
728 annual sea ice retreat and advance and their relation to El Niño-Southern Oscillation and

- 729 Southern Annular Mode variability. *Journal of Geophysical Research: Oceans*, 113(3), 1–20.  
730 <https://doi.org/10.1029/2007jc004269>
- 731 Stolarski, R. S., McPeters, R. D., & Newman, P. a. (2005). The Ozone Hole of 2002 as Measured by  
732 TOMS. *Journal of the Atmospheric Sciences*, 62(3), 716–720. [https://doi.org/10.1175/JAS-](https://doi.org/10.1175/JAS-3338.1)  
733 3338.1
- 734 Stone, K. A., Solomon, S., Kinnison, D. E., & Mills, M. J. (2021). On Recent Large Antarctic Ozone  
735 Holes and Ozone Recovery Metrics. *Geophysical Research Letters*, 48(22).  
736 <https://doi.org/10.1029/2021GL095232>
- 737 Thompson, D. W. J., Baldwin, M. P., & Solomon, S. (2005). Stratosphere–troposphere coupling in the  
738 Southern Hemisphere. *Journal of the Atmospheric Sciences*, 62(3), 708–715.  
739 <https://doi.org/10.1175/JAS-3321.1>
- 740 Thompson, D. W. J., & Wallace, J. M. (2000). Annular modes in the extratropical circulation. Part I:  
741 Month-to-month variability. *Journal of Climate*, 13(5), 1000–1016.  
742 [https://doi.org/10.1175/1520-0442\(2000\)013<1000:AMITEC>2.0.CO;2](https://doi.org/10.1175/1520-0442(2000)013<1000:AMITEC>2.0.CO;2)
- 743 Walters, D., Boutle, I., Brooks, M., Melvin, T., Stratton, R., Vosper, S., Wells, H., Williams, K.,  
744 Wood, N., Allen, T., Bushell, A., Copsey, D., Earnshaw, P., Edwards, J., Gross, M., Hardiman,  
745 S., Harris, C., Heming, J., Klingaman, N., ... Xavier, P. (2017). The Met Office Unified Model  
746 Global Atmosphere 6.0/6.1 and JULES Global Land 6.0/6.1 configurations. *Geoscientific Model*  
747 *Development*, 10(4), 1487–1520. <https://doi.org/10.5194/gmd-10-1487-2017>
- 748 Wang, G., Hendon, H. H., Arblaster, J. M., Lim, E. P., Abhik, S., & van Rensch, P. (2019).  
749 Compounding tropical and stratospheric forcing of the record low Antarctic sea-ice in 2016.  
750 *Nature Communications*, 10(1), 13. <https://doi.org/10.1038/s41467-018-07689-7>
- 751 Wargan, K., Weir, B., Manney, G. L., Cohn, S. E., & Livesey, N. J. (2020). The Anomalous 2019  
752 Antarctic Ozone Hole in the GEOS Constituent Data Assimilation System With MLS  
753 Observations. *Journal of Geophysical Research: Atmospheres*, 125(18), 1–28.  
754 <https://doi.org/10.1029/2020JD033335>
- 755 Waters, J., Lea, D. J., Martin, M. J., Mirouze, I., Weaver, A., & While, J. (2015). Implementing a  
756 variational data assimilation system in an operational 1/4 degree global ocean model. *Quarterly*  
757 *Journal of the Royal Meteorological Society*, 141(687), 333–349.  
758 <https://doi.org/10.1002/qj.2388>
- 759 Waters, J. W., Froidevaux, L., Harwood, R. S., Jarnot, R. F., Pickett, H. M., Read, W. G., Siegel, P.  
760 H., Cofield, R. E., Filipiak, M. J., Flower, D. A., Holden, J. R., Lau, G. K., Livesey, N. J.,  
761 Manney, G. L., Pumphrey, H. C., Santee, M. L., Wu, D. L., Cuddy, D. T., Lay, R. R., ... Walch,

762 M. J. (2006). The Earth observing system microwave limb sounder (EOS MLS) on the aura  
763 Satellite. *IEEE Transactions on Geoscience and Remote Sensing*, 44(5), 1075–1092.  
764 <https://doi.org/10.1109/TGRS.2006.873771>

765 Wedd, R., Alves, O., de Burgh-Day, C., Down, C., Griffiths, M., Hendon, H. H., Hudson, D., Li, S.,  
766 Lim, E.-P., Marshall, A. G., Shi, L., Smith, P., Smith, G., Spillman, C. M., Wang, G., Wheeler,  
767 M. C., Yan, H., Yin, Y., Young, G., ... Zhou, X. (2022). ACCESS-S2: the upgraded Bureau of  
768 Meteorology multi-week to seasonal prediction system. *Journal of Southern Hemisphere Earth  
769 Systems Science*, 72(3), 218–242. <https://doi.org/10.1071/ES22026>

770 Yook, S., Thompson, D. W. J., & Solomon, S. (2022). Climate Impacts and Potential Drivers of the  
771 Unprecedented Antarctic Ozone Holes of 2020 and 2021. *Geophysical Research Letters*, 49(10).  
772 <https://doi.org/10.1029/2022gl098064>

773 Yu, P., Davis, S. M., Toon, O. B., Portmann, R. W., Bardeen, C. G., Barnes, J. E., Telg, H., Maloney,  
774 C., & Rosenlof, K. H. (2021). Persistent Stratospheric Warming Due to 2019–2020 Australian  
775 Wildfire Smoke - Supplementary Information. *Geophysical Research Letters*, 48(7).  
776 <https://doi.org/10.1029/2021GL092609>

777 Yuan Zhang, Wallace, J. M., & Battisti, D. S. (1997). ENSO-like interdecadal variability: 1900-93.  
778 *Journal of Climate*, 10(5), 1004–1020. [https://doi.org/10.1175/1520-  
779 0442\(1997\)010<1004:eliv>2.0.co;2](https://doi.org/10.1175/1520-0442(1997)010<1004:eliv>2.0.co;2)

780

**Predictability of the 2020 Antarctic strong vortex event and the role of ozone forcing**

Eun-Pa Lim<sup>1</sup>, Linjing Zhou<sup>1</sup>, Griffith Young<sup>1</sup>, S. Abhik<sup>2</sup>, Irina Rudeva<sup>1</sup>, Pandora Hope<sup>1</sup>,  
Matthew C. Wheeler<sup>1</sup>, Julie M. Arblaster<sup>2</sup>, Harry H. Hendon<sup>2</sup>, Gloria L. Manney<sup>3,4</sup>,  
Seok-Woo Son<sup>5</sup>, and Jiyoung Oh<sup>6</sup>

<sup>1</sup> Eun-Pa Lim<sup>1</sup>, Linjing Zhou<sup>1</sup>, Griffith Young<sup>1</sup>, S. Abhik<sup>2</sup>, Irina Rudeva<sup>1</sup>, Pandora Hope<sup>1</sup>, Matthew C. Wheeler<sup>1</sup>, Julie M. Arblaster<sup>3</sup>, Harry H. Hendon<sup>3</sup>, Gloria L. Manney<sup>4,5</sup>, Seok-Woo Son<sup>6</sup>, Jiyoung Oh<sup>7</sup>

<sup>1</sup> Bureau of Meteorology, Melbourne, Victoria, Australia

<sup>2</sup> School of Earth, Atmosphere and Environment, Monash University, Clayton, Victoria, Australia

<sup>3</sup> Securing Antarctica's Environmental Future, School of Earth, Atmosphere and Environment, Monash University, Clayton, Victoria, Australia

<sup>4</sup> NorthWest Research Associates, Socorro, New Mexico, USA

<sup>5</sup> Department of Physics, New Mexico Institute of Mining and Technology, Socorro, New Mexico, USA

<sup>6</sup> School of Earth and Environmental Sciences, Seoul National University, Seoul, Republic of Korea

<sup>7</sup> Korea Meteorological Administration, Seoul, Republic of Korea

**Contents of this file**

Figures S1 to S5

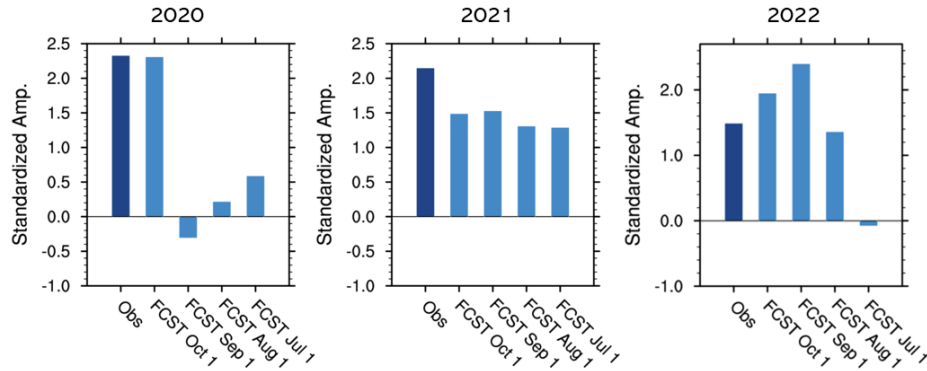


**Figure S1.** The Bureau of Meteorology (BoM)'s dynamical forecasts for the October-December mean stratospheric polar vortex of the SH ( $[U]'$  at 60°S, 10 hPa) for 2020, 2021 and 2022. The 2020 and 2021 events were predicted by ACCESS-S1 and the 2022 event was predicted by ACCESS-S2 because ACCESS-S2 became operational at the BoM in October 2021. The dark blue bars indicate the observed strengths of the vortices, and the light blue bars show the forecast strengths as a function of forecast start date as denoted on the x-axis. The observed and forecast standardized anomalies were obtained relative to their respective climatological means and standard deviations of 1990-2012 when ACCESS-S1 hindcasts are available. This figure shows that the 2021 and 2022 strong vortex events during the October-December season were predictable from the beginning of August (i.e., 2-month lead time), whereas the 2020 strong vortex event was only predictable from the beginning of October (i.e., zero lead time).

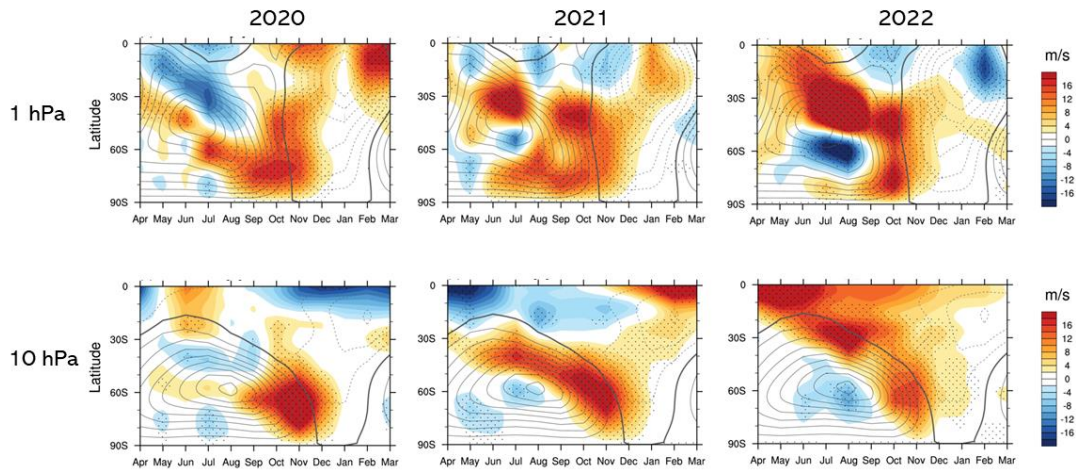


**Figure S2.** Zonal-mean zonal wind anomalies ( $[U]$ ) at 1 hPa (upper panels) and 10 hPa (lower panels) for 2020, 2021 and 2022. Contours indicate the 1981-2018 climatologies of the zonal-mean zonal winds at the 1 and 10 hPa levels with 10 ms<sup>-1</sup> intervals. Stippling indicates anomalies greater than 1 standard deviation estimated over the climatological period. The 2021 and 2022 strong vortex events over Antarctica observed from October to December at 10 hPa were associated with equatorward shifts of the winter stratospheric jet and subsequent poleward movements of increased westerly anomalies in the midlatitudes, which is consistent with the historical relationship of zonal-mean zonal wind anomalies associated with strong polar vortex events in 1981-2018 (main article Figure 3c). On the other hand, the winter to spring evolution of the 2020 strong vortex was different from those of the 2021 and 2022 events or that of the historical pattern.

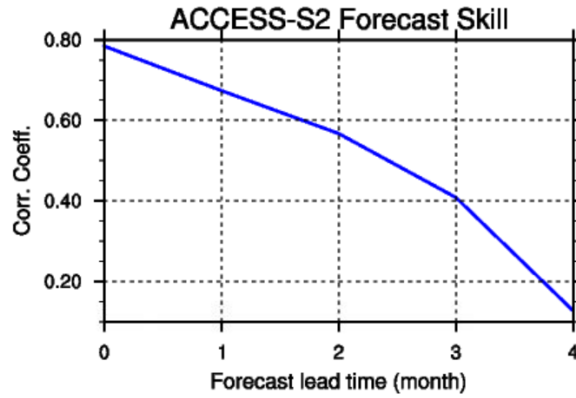


**Figure S3.** ACCESS-S2 hindcast (retrospective forecast) skill for the October-December mean stratospheric polar vortex of the SH monitored by [U]' at 60°S and 10 hPa. The 9-member ensemble mean forecasts as used in Wedd et al. (2022) were verified against the index derived from the JRA-55 reanalysis for 1981-2018. Correlation coefficients greater than 0.3 are statistically significant at the 95% confidence level, as assessed by a one-tailed student t-test given 38 samples.

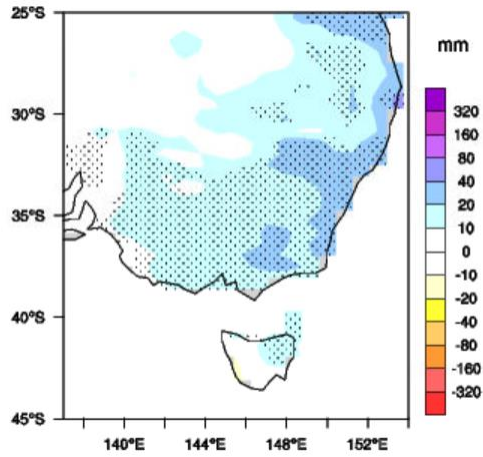


**Figure S4.** The rainfall and SAM relationship in December-January-February simulated in ACCESS-S2 hindcasts over 1981-2018 at 3-month lead time. The forecast SAM index was obtained by projecting the forecast 700-hPa geopotential height (GPH) anomaly data onto the pattern of the leading EOF mode of the observed variability of the 700-hPa GPH poleward of 20°S, which was derived using the JRA-55 reanalysis data and is displayed in Figure S5. Stippling indicates the statistical significance on the regression coefficients at the 90% confidence level, assessed by a two-tailed student t-test with 38 samples.

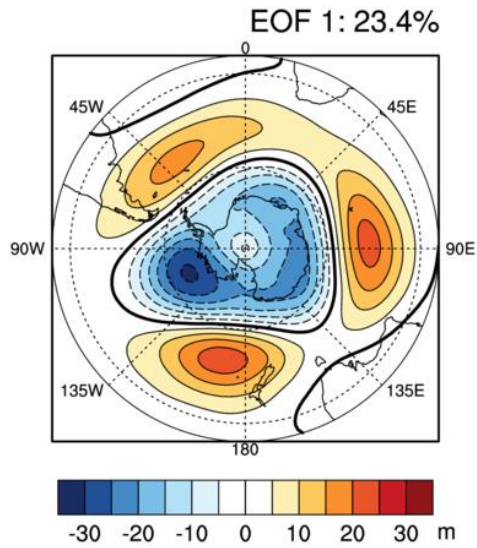


**Figure S5.** JRA-55 monthly 700-hPa GPH anomalies regressed onto the standardized time series of the 1st EOF mode of variability of monthly mean 700-hPa GPH, following (Thompson & Wallace, 2000). The EOF analysis was performed on the GPH anomalies weighted by squared cosine latitude over the domain of 20–90°S in the period of 1981–2018. The GPH anomaly pattern associated with the positive index polarity of the SAM is displayed, and the explained variance by this mode is shown in the top right corner of the figure.